

Probing the ionizing photon output of galaxies near cosmic dawn with the patchy kSZ effect

Garett Lopez,^a Anson D’Aloisio,^a and Christopher Cain^b

^aDepartment of Physics and Astronomy, University of California, Riverside,
900 University Ave., Riverside, CA, 92521, USA

^bSchool of Earth and Space exploration, Arizona State University
Tempe, AZ 85281, USA

E-mail: garett.lopez@ucr.edu, ansond@ucr.edu, clcain3@asu.edu

Abstract. A key result from JWST’s first cycles is that galaxy formation was well underway by $z = 10$. The implications of these early galaxies for reionization are less clear, however. The CMB is one of the few windows into the ionization state of the IGM during reionization’s first half, providing an important probe of the ionizing photon sources at those times. Meanwhile, measurements of the Lyman- α forest in the spectra of high- z quasars have improved to the level of tightly constraining the timing of reionization’s end. In this paper, we use radiative transfer simulations to explore how measurements of the patchy kinetic Sunyaev Zel’dovich (pkSZ) effect, when combined with Lyman- α forest measurements, can be used to constrain the early stages of reionization and the nature of its sources. For a given source model, we find that the amplitude of the pkSZ power spectra strongly correlates with the start time of reionization, and constrains the number of ionizing photons produced by the high- z source population. Allowing for variations in the source model, this correlation is weakened by a degeneracy between the reionization history and the effects of source clustering. However, we demonstrate two potential ways of breaking this degeneracy using: (1) measurements of large-scale fluctuations in the Ly α forest opacity at $z = 5 - 6$, and/or; (2) the shape of the pkSZ power spectrum measured in future CMB surveys. Models with highly clustered sources yield steeper slopes in the pkSZ power around $\ell = 3,000$, so measurements at additional angular scales can be used to break the history-clustering degeneracy. Our results highlight how future pkSZ measurements will complement JWST observations to improve our understanding of the ionizing sources near cosmic dawn.

Keywords: Sunyaev-Zeldovich effect; intergalactic media; reionization; high redshift galaxies

Contents

1	Introduction	1
2	Methods	3
2.1	Radiative Transfer Simulations of Reionization	3
2.2	The kinetic Sunyaev-Zel’dovich Angular Power Spectrum	5
3	Sensitivity of pkSZ Power to the Beginning of Reionization	7
3.1	Models	7
3.2	Results	8
3.2.1	The Starting Epoch of Reionization	8
3.2.2	Ionizing Photon Production of Early Galaxies	11
4	Effect of Source Clustering on pkSZ Power	13
4.1	Quantifying the Effect of Source Clustering	13
4.2	Breaking the Degeneracy with Source Clustering	15
4.2.1	The Ly α Forest Opacity Fluctuations	17
4.2.2	The Shape of the pkSZ Power Spectrum	18
5	Discussion	21
5.1	Models with evolving emissivity-halo connection	21
5.2	Stochastic Star Formation	22
5.3	Comparison to Previous Results	25
6	Conclusion	26
A	Comparing pkSZ for Full and Reduced Speed of Light Runs	27

1 Introduction

Over the past decade, quasar absorption spectra measurements have sharpened our understanding of reionization’s last phases. A number of lines of evidence point to the last $\lesssim 20\%$ of reionization occurring at $z < 6$. These include the observed evolution in the Lyman- α (Ly α) forest mean flux and large-scale opacity fluctuations [1–3], dark gap statistics of the co-eval Ly α and Ly β forests [4, 5], and rapid evolution in the mean free path of ionizing photons between $z = 5–6$ [6–11]. Most recently, Refs. [12–14] reported evidence of damping wings at the edges of dark gaps in the co-eval Ly α and Ly β forests at $z < 6$, so far the most direct indication of ongoing reionization at those times. In combination, these measurements have moved beyond providing just a lower bound in redshift for the end of reionization; they constrain the timing of it [8, 15–17]. The central focus of the current paper is how this constraint alters the interpretation of existing and future measurements of the kinetic Sunyaev-Zel’dovich (kSZ) signal from reionization.

Comparatively little is known about reionization’s earliest phases. With the wavelength coverage and spectroscopy provided by the Near Infrared Camera and Spectrometer (NIRCam and NIRSpec), the James Webb Space Telescope (JWST) promises groundbreaking insights

into the earliest sources of reionization. JWST observations have already provided measurements of the cosmic rest-frame ultraviolet (UV) luminosity density (ρ_{UV}) at redshifts up to $z \sim 14$ [18–26]. These early studies have not yet converged on a coherent picture, likely owing to sample variance and/or low redshift interlopers [e.g. 19, 25, 27]. In aggregate, they make clear that galaxies were forming just a few hundred million years after the Big Bang. The implications of these observations for reionization, however, are less clear. The ionizing emissivity, or number of ionizing photons per unit comoving volume emitted into the intergalactic medium (IGM) at redshift z , is often modeled with the ansatz

$$\dot{N}_{\text{ion}} = \langle f_{\text{esc}} \xi_{\text{ion}} \rangle \cdot \rho_{\text{UV}}, \quad (1.1)$$

where f_{esc} is the escape fraction of ionizing photons, and ξ_{ion} is the ionizing efficiency, the conversion factor between a galaxy’s non-ionizing UV luminosity and its rate of hydrogen-ionizing photon production.¹ The brackets denote a UV-luminosity-weighted average over the galaxy population. With JWST, ionizing efficiencies have been measured for samples of up to a few dozen galaxies at $z > 5$ [28–30]. Again, the conclusions of these early studies are varied, with some reporting a factor of a few enhancement in ξ_{ion} over the value of $\log_{10}(\xi_{\text{ion}}/\text{erg Hz}^{-1}) = 25.2$ commonly adopted before JWST (e.g. [31]). The variation among these early results could be a result of redshift evolution and/or a correlation between ξ_{ion} and UV luminosity [28–30].

But even if we had a precise empirical model for ξ_{ion} and its main dependencies, the implications for reionization would still be difficult to glean for two reasons: (1) it is impossible to measure f_{esc} directly at these redshifts owing to the prohibitively large opacity of the IGM to ionizing photons; (2) much of the ionizing photon budget could have been sourced by galaxies too faint to be detected by JWST [e.g. 26, 32, 33]. Indeed, Ref. [34] attempted to hash out the implications of the recent JWST results for reionization. They argued that even the *observed* high- z galaxies with $M_{\text{UV}} < -15$ should have been prolific producers and leakers of ionizing photons; so much so that reionization would have completed well before $z = 6$, in violation of Ly α forest constraints. Their argument, however, relies on a model for f_{esc} that is based on a correlation between f_{esc} and UV-continuum slope measured at $z \sim 0$ [35], and a measurement of ξ_{ion} reported by Ref. [30], which is likely biased high by selection effects [36]. This discussion serves to highlight the large uncertainties still at play when attempting to infer the ionizing output of high- z galaxies from their non-ionizing spectral properties (see also the detailed discussion of these nuances in Ref. [37]).

Constraints on the ionization state of the IGM are a critical indirect probe of the ionizing emissivity of the galaxy population. Unfortunately, at $z > 8$, such constraints are still limited. To date, 21 cm experiments targeting the epoch of reionization have placed only upper limits on the $z \geq 8$ power spectrum [38, 39]. Observations of Ly α emission in high- z galaxy spectra have begun to place constraints on reionization’s early stages [e.g. 40–42], but these are limited by poor statistics and model dependence [43]. The cosmic microwave background (CMB) provides integral constraints that stem from measurements of the EE power spectrum at low ℓ and from the contribution of reionization to the kSZ effect, the so-called patchy kSZ contribution (pkSZ)². The former is typically expressed as the summary statistic τ_{es} , the electron scattering optical depth, although additional information is contained in the detailed shape of the EE power. Measurements of τ_{es} have almost always been interpreted

¹The non-ionizing UV luminosity of a galaxy is typically measured at rest-frame 1500 Å.

²In some works this is also termed the “reionization kSZ” or rkSZ.

as a constraint on reionization’s midpoint. Ref. [17] recently pointed out that when τ_{es} is combined with Ly α forest constraints on the end of reionization, it becomes a measurement of reionization’s *duration*. Perhaps this could be exploited to glean insights into reionization’s early phases. However, given the low value of $\tau_{\text{es}} = 0.058 \pm 0.0062$ measured from Planck data [44, 45], the results of Ref. [46] suggest that even a cosmic-variance limited measurement of the low- ℓ EE power would be unlikely to discriminate between realistic models.

The pkSZ signal provides an alternative path forward. Ref. [47] reported a $\geq 3\sigma$ detection of the total kSZ power at $\ell = 3,000$, of $D_{3000} = 3.0 \pm 1.0 \mu\text{K}^2$ from the South Pole Telescope (SPT). They measured the pkSZ component to be $D_{3000}^{\text{pkSZ}} = 1.1_{-0.7}^{+1.0} \mu\text{K}^2$ using estimates of the post-reionization contribution from [48, 49]. During the preparation of this manuscript, Ref. [50] measured a total kSZ power of $D_{3000} = 1.48_{-1.10}^{+0.71} \mu\text{K}^2$ with the Atacama Cosmology Telescope (ACT).³ Forthcoming experiments such as Simon’s Observatory and CMB-S4 Wide are forecasted to measure D_{3000}^{pkSZ} to a precision of $\sim \pm 0.2 \mu\text{K}^2$ ($1\text{-}\sigma$ limits), improving to $\sim \pm 0.1 \mu\text{K}^2$ when combined with future LiteBIRD constraints on τ_{es} [51]. In this paper, we use radiative transfer simulations of reionization to explore what measurements of the pkSZ power could tell us about the beginning of reionization and the ionizing emissions of the earliest galaxies observed by JWST. Another important (and related) question concerns the clustering of the ionizing sources. From an empirical perspective, essentially nothing is known about the source-halo connection at this epoch. The pkSZ power is in principle sensitive to the morphology of reionization, which is shaped by the clustering of its sources. It may thus contain precious information about the dark matter halos in which early ionizing sources resided. In this paper, we take up the question of whether pkSZ measurements could inform us about the galaxy-halo connection of the ionizing sources that began reionization. As stated above, a key focus of this paper is to incorporate the most recent developments in our understanding of reionization’s last phases into the discussion of how to interpret the pkSZ signal. As we will show, pinning down the end of reionization with Ly α forest measurements improves our ability to draw conclusions about the start of reionization.

The remainder of this paper is organized as follows. In §2, we describe our simulation methods. In §3, we explore using the pkSZ power to probe the starting epoch of reionization and the high- z ionizing emissivity. In §4, we consider what the power can tell us about the clustering of the earliest ionizing sources. In §5, we discuss the dependence of our results on modeling assumptions and compare our results to other works in the literature. We offer concluding remarks in §6. In all calculations, we adopt a flat Λ CDM cosmology with $\Omega_m = 0.305$, $\Omega_b = 0.048226$, $H_0 = 68$ km/s/Mpc, $\sigma_8 = 0.82033$, and $n_s = 0.9667$.

2 Methods

2.1 Radiative Transfer Simulations of Reionization

We have run a suite of radiative transfer (RT) simulations with the FLEXRT code of Ref. [52]. We refer the reader to their paper for a detailed description of the main RT engine. Briefly, the code employs an adaptive ray tracing algorithm based on the Healpix RT formalism of Ref. [53], and a ray merging scheme akin to that of Ref. [54] for increased speed. FLEXRT adds to this a detailed sub-grid model for the LyC opacity of the IGM, described in Refs. [55, 56], as well as the reionization I-front heating model of Ref. [57]. The RT was run in

³Ref. [50] did not report a pkSZ measurement. For reference, adopting a conservative (low) estimate of $0.85 \mu\text{K}^2$ for the post-reionization contribution to the kSZ power from Ref. [49] yields a 2σ upper limit on the pkSZ power of $D_{3000}^{\text{pkSZ}} \lesssim 2.05 \mu\text{K}^2$.

post-processing on the cosmological hydrodynamics simulation from Ref. [58], which was run with the Eulerian code of Ref. [59]. The box size is $L_{\text{box}} = 200 h^{-1}$ cMpc and the simulation contains 2×2048^3 dark matter and gas resolution elements. Ref. [60] recently improved the halo mass resolution over that of Ref. [58] by running with the same initial conditions an N-body-only simulation using $N = 3600^3$ particles. Dark matter halos were identified using the spherical over-density method described in [61]. We find that the halo mass function in our simulation agrees with the halo mass function of Ref. [61] to within 10 % down to a halo mass of $3 \times 10^9 h^{-1} M_{\odot}$. However, in order to maximize the number of sources at $z > 10$ in our simulations, we use all halos down to a mass of $10^9 h^{-1} M_{\odot}$. At this mass, the simulated halo mass functions are suppressed by as much as $\sim 50\%$ with respect to the fits in Ref. [61]. We note that: (1) in reality, the cutoff in the ionizing sources induced by feedback/inefficient star formation is not perfectly sharp. In some sense, the incompleteness of the mass function crudely mimics a smoother decline; (2) the halos near this threshold are subdominant in their contribution to the total ionizing photon budget in our most realistic source models (c.f. Fig. 1 of Ref. [62]).

We populate the dark matter halos with ionizing sources by first abundance matching to the observed rest-frame UV luminosity function. We use the luminosity function measurements of Ref. [63] at $z < 8$, Ref. [64] at $8 < z < 14$, and Ref. [65] at $z = 14.5$. We extrapolate the luminosity function of [65] out to $z = 18$, the starting epoch of our simulations. In the ensuing sections we describe our source modeling in detail, i.e. how exactly we assign ionizing emissivities to halos. The RT is performed on a uniform grid of size $N_{\text{RT}} = 200^3$. For computational speed, we adopt the monochromatic approximation with photon energies $E_{\gamma} = 19$ eV. This energy is chosen to yield the same frequency-averaged hydrogen photoionization cross section as a power-law spectrum $I_{\nu} \propto \nu^{-1.5}$ between 1 and 4 Ry, where I_{ν} is the specific intensity. This power-law spectrum approximates calculations of the time-averaged spectrum of metal poor stellar populations in synthesis models [e.g. 57]. We run the RT from $z = 18$ down to $z = 4.8$.

A key aspect of this work is the empirical calibration of our simulations to the observed Ly α forest mean transmission at $5 \lesssim z \lesssim 6$. For this task we simulate the Ly α forest along 4,000 skewers traced at random directions from random locations in our hydrodynamic simulation volume (with $L_{\text{box}} = 200 h^{-1}$ Mpc and $N = 2048^3$ gas resolution elements). The gas properties on these skewers are rescaled to the RT grid values under the assumption of photoionization equilibrium, which is almost always a good approximation in the reionized IGM owing to the short photoionization equilibration timescale of the hydrogen gas. For computing the Ly α optical depth, we employ the widely used approximation to the Voigt profile of Ref. [66]. We apply two resolution corrections to the simulated mean flux: (1) the convergence correction described in the appendix of Ref. [58], which approximately corrects for spurious opacity in voids owing to the finite resolution of the hydrodynamic simulation; (2) the temperature-density correction described in the appendix of Ref. [60], which assigns a sub-grid temperature-density relation to each RT cell based on its local reionization redshift. This corrects for the relatively large cell sizes of our RT grid compared to the higher resolution of the hydrodynamic simulation. We refer the reader to those papers for detailed descriptions.

To calibrate each simulation, we adjust the global ionizing emissivity – particularly at $z \lesssim 7$ – by trial and error until the simulated mean Ly α forest transmission agrees with observational measurements. This is equivalent to adjusting $\langle f_{\text{esc}} \xi_{\text{ion}} \rangle$ as a function of redshift at $z \lesssim 7$. (Plots illustrating this procedure, including the empirical constraints used, will be presented below.) This procedure would be extremely time consuming for the dozens

of models explored in this paper, as each model requires at least several trial runs. The reduced speed of light approximation is a commonly used method to reduce computational cost. However, previous works have shown that it can lead to significant inaccuracies in the intensity and structure of the ionizing radiation background, particularly near the end of reionization [60, 67, 68]. Fortunately, Ref. [69] developed a rescaling/correction procedure that allows us to use the reduced speed of light approximation without sacrificing accuracy for the quantities of interest, greatly increasing the speed of the calibration and making this work tractable. The following equation, motivated and tested by [69], relates the global ionizing emissivity in a simulation with full speed of light, \dot{N}_{ion}^c , to that in a simulation using reduced speed of light, $\dot{N}_{\text{ion}}^{\tilde{c}}$,

$$\dot{N}_{\text{ion}}^c(t) = \dot{N}_{\text{ion}}^{\tilde{c}} - \dot{N}_{\gamma}^{\tilde{c}} \left(1 - \frac{\tilde{c}}{c}\right), \quad (2.1)$$

where $\tilde{c}/c < 1$ is the ratio of the reduced speed of light to the speed of light, c . The quantity $N_{\gamma}^{\tilde{c}}$ is the mean number density of ionizing photons in the simulation with reduced speed of light, i.e.

$$N_{\gamma}^{\tilde{c}} = \int_0^t dt \left[\dot{N}_{\text{ion}}^{\tilde{c}} - \dot{N}_{\text{abs}}^{\tilde{c}} \right], \quad (2.2)$$

where $\dot{N}_{\text{abs}}^{\tilde{c}}$ is the total absorption rate per unit volume. Given a simulation with reduced speed of light \tilde{c} , we can use equations (2.1) and (2.2) to map the quantities $\dot{N}_{\text{ion}}^{\tilde{c}}(t)$ and $N_{\gamma}^{\tilde{c}}(t)$ to $\dot{N}_{\text{ion}}^c(t)$, giving approximately the emissivity history that would be needed in a simulation with full speed of light to produce the same reionization history, morphology, and key observables. In practice, Ref. [69] showed that these equations recover the large-scale morphology and Ly α forest mean flux of a full-speed-of-light simulation to within 20% for simulations with $\tilde{c}/c \geq 0.2$ (the accuracy increases substantially with increasing \tilde{c}/c); the global reionization history is recovered to within 1% for \tilde{c}/c as low as 0.05. In what follows, all of our simulations use $\tilde{c}/c = 0.2$. We employ equations (2.1) and (2.2) to map our emissivities to what they would be in a simulation with full speed of light. All emissivities plotted in this paper correspond to \dot{N}_{ion}^c . We further test this rescaling procedure for the application at hand in Appendix A. We compare the pkSZ power between full-speed-of-light-runs and reduced-speed-of-light-runs with $\tilde{c}/c = 0.2$. We find that the above procedure recovers the pkSZ power spectra from full-speed-of-light runs to within 1.5%, validating our approach. We emphasize that the dozens of calibrated RT simulations run for this paper would have been a factor of $\approx 5\times$ more expensive without this time-saving (yet accurate) method.

2.2 The kinetic Sunyaev-Zel'dovich Angular Power Spectrum

The temperature anisotropy induced by the kSZ effect can be expressed as the line-of-sight integral [70],

$$\frac{\Delta T}{T} = -\sigma_T \bar{n}_{e,0} \int e^{-\tau_{\text{es}}} \frac{\hat{\gamma} \cdot \vec{q}}{c} \frac{ds}{a^2}, \quad (2.3)$$

where $\hat{\gamma}$ is a unit vector along the line of sight, σ_T is the Thompson scattering cross section, $\bar{n}_{e,0}$ is the co-moving mean electron density, a is the cosmological scale factor, and s is the co-moving distance. The central quantity is the ionized momentum, $\vec{q} = (1 + \delta)\chi\vec{v}$, where δ is the matter density contrast (with zero mean), $\chi = n_e/(n_H + 2n_{He})$ is the free electron fraction, and \vec{v} is the peculiar velocity. In this work we assume that the first reionization of

helium traces hydrogen reionization and the second reionization of helium occurs instantly at $z=3$, although our results are insensitive to this choice. We compute the pkSZ angular power spectrum using the method of Ref. [71], which expresses the power as

$$C_\ell = \left(\frac{\sigma_T \bar{n}_{e,0}}{c} \right)^2 \int \frac{ds}{s^2 a^4} e^{-2\tau} \frac{P_{q_\perp}(k = \ell/s, s)}{2}, \quad (2.4)$$

where $(2\pi)^3 P_{q_\perp}(k) \delta^D(\vec{k} - \vec{k}') = \langle \tilde{q}_\perp(\vec{k}) \cdot \tilde{q}_\perp^*(\vec{k}') \rangle$ is the power spectrum of the ionized momentum modes perpendicular to the Fourier wave vector, $\tilde{q}_\perp = \tilde{q} - \hat{k}(\tilde{q} \cdot \hat{k})$ (the so-called ‘‘transverse’’ modes), and $\delta^D(\vec{k} - \vec{k}')$ is the Dirac-delta function. Note that $\tilde{q} = \int \vec{q} e^{-i\vec{k} \cdot \vec{q}} d^3\vec{x}$ denotes the Fourier transform of \vec{q} . Only the \tilde{q}_\perp modes contribute significantly to the kSZ signal owing to the \tilde{q}_\parallel contributions canceling out in the line-of-sight integral. (See Refs. [71, 72] for a discussion.)

In general, it is common to write the angular power spectrum in the dimensionless form: $D_\ell = C_\ell(\ell + 1)\ell/(2\pi)$. For the most part, we will focus on the pkSZ power at $\ell = 3000$ (D_{3000}^{pkSZ}). This is the angular scale of existing measurements due to the primary CMB strongly dominating at $\ell \lesssim 3000$, and other foregrounds becoming increasingly problematic at $\ell \gtrsim 3000$. Ref. [51] forecasts that future experiments such as the Simons Observatory and CMB-S4 may be able to extend kSZ measurements to multiple bins in $\ell \in [2500, 5000]$. As we will show in §4, the ℓ -dependence of the power contains information about the clustering of reionization sources, so probing the power at several ℓ could be highly informative.

Running RT simulations imposes practical limitations on the volume of our box. With our modest box sizes of $L_{\text{box}} = 200 h^{-1} \text{cMpc}$, we miss large-scale velocity modes that are known to source kSZ power. To compensate for this, we add the correction term to P_{q_\perp} developed by Ref. [71],

$$P_{q_\perp}^{\text{miss}}(k, z) = \int_{k < k_{\text{box}}} \frac{d^3 k'}{(2\pi)^3} (1 - \mu^2) P_{\chi(1+\delta)}(|\vec{k} - \vec{k}'|) P_{vv}^{\text{lin}}(k') \quad (2.5)$$

where $k_{\text{box}} = 2\pi/L_{\text{box}}$ is the box-scale wave number, $\mu = \hat{k} \cdot \hat{k}'$, $P_{\chi(1+\delta)}(k)$ is the ionized matter power spectrum and $P_{vv}^{\text{lin}}(k)$ is the linear velocity power spectrum, which we evaluate using CAMB [73]. Ref. [74] found that equation (2.5) may nonetheless lead to an underestimate of D_{3000}^{pkSZ} by $\sim 10\text{-}20\%$ because the non-Gaussianity of reionization renders the irreducible component of $\langle \delta_\chi v \cdot \delta_\chi v \rangle$ non-negligible. This does not affect our broad conclusions, however.

The above integrals can be broken up into two contributions: (1) the so-called homogeneous kinetic Sunyaev-Zel’dovich Effect (hkSZ) from the post-reionization IGM; (2) the patchy kinetic Sunyaev-Zel’dovich Effect (pkSZ) sourced by reionization – the quantity of interest here. Measurements of the pkSZ component require subtracting the hkSZ power. For simplicity, and because reionization ends as late as $z_{\text{end}} \approx 5$ in some of our models, we define the pkSZ power to be the contribution from $z > 5$, even for models in which reionization ends significantly earlier than $z = 5$. We note that the measurement of Ref. [75], against which we will compare our models, adopts a slightly different demarcation of $z_{\text{end}} = 5.5$. Using the scaling relationships in Ref. [76], we find that rescaling the measurement to $z_{\text{end}} = 5$ would increase the inferred pkSZ power by $\sim 0.1 \mu\text{K}^2$ (by decreasing the hkSZ power for a fixed total kSZ). This is a relatively small effect that would not change our conclusions.

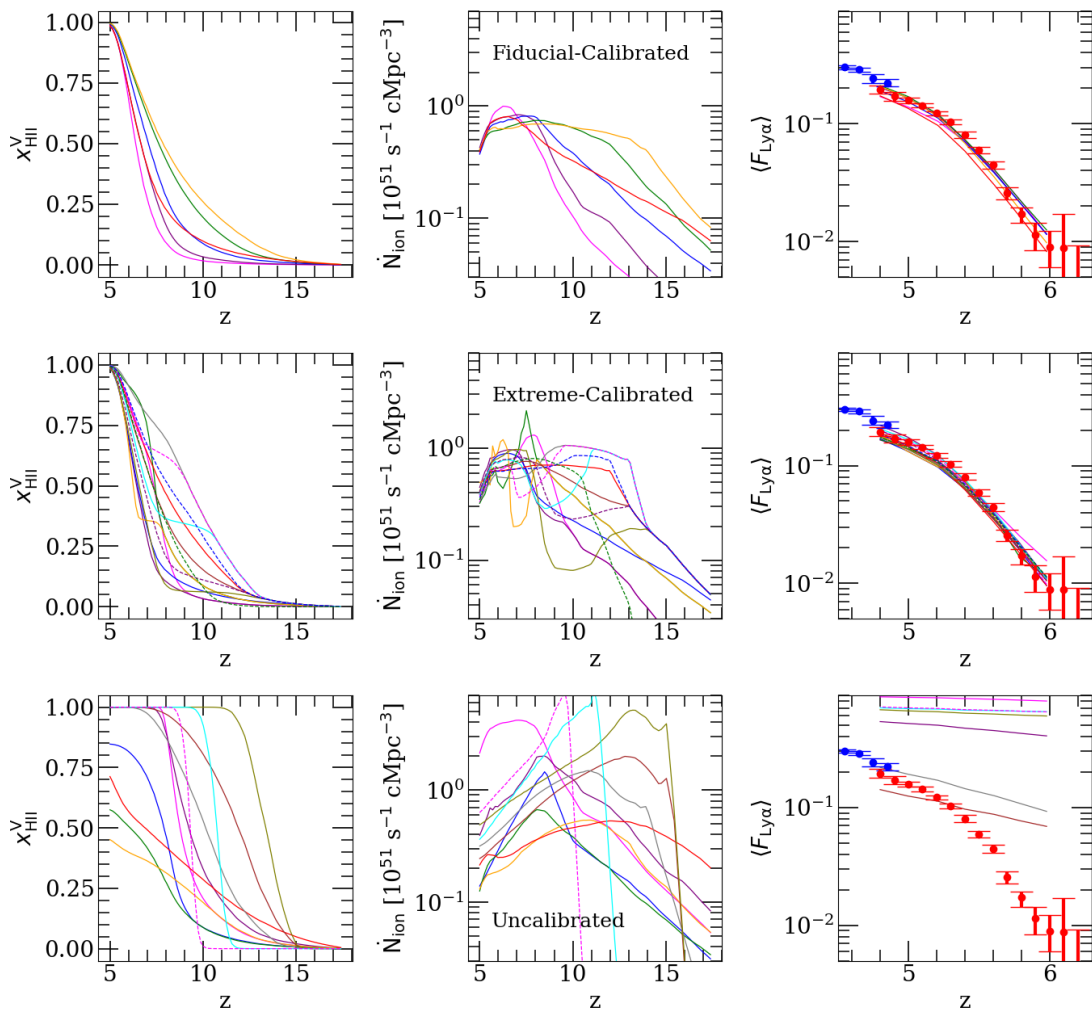


Figure 1. Summary of reionization models used in §3: the volume-weighted ionized fraction (left column), ionizing emissivity histories (center column), and forest transmission fraction (right column). The emissivities of the calibrated models are tuned for agreement with the observational measurements of Refs. [15], shown as the red data points in the right column. For reference, the blue data points show the lower redshift measurements of Ref. [77]. FIDUCIAL-CALIBRATED models (top row) complete reionization in a manner consistent with the forest transmission fraction constraints, and have smooth/physical emissivity histories. The EXTREME-CALIBRATED models have un-physically rapid and/or non-monotonic evolution in the emissivity. UNCALIBRATED models (bottom row) complete reionization far too early or late to agree with the Ly α forest constraints. The EXTREME-CALIBRATED and UNCALIBRATED models are for illustrative purposes only; they are used to test the generality of our main results below.

3 Sensitivity of pkSZ Power to the Beginning of Reionization

3.1 Models

In this section, we adopt a source model in which the ionizing emissivity of a galaxy is assumed proportional to its rest-frame UV luminosity, $\dot{n}_{\text{ion}} \propto L_{\text{UV}}$. Since the UV-luminosity of a galaxy is uniquely mapped to a halo mass through abundance matching, we refer to this as

the “emissivity-halo” prescription. The emissivity-halo prescription sets the clustering of the ionizing sources, which, in turn, shapes the morphology of reionization. The current section focuses on what the pkSZ power can tell us about the ionizing output of high- z galaxies *for a fixed emissivity-halo prescription*. In §4, we will explore how changing the model (thus changing morphology of reionization) affects our results. Note that, although we fix the emissivity-halo prescription, we still vary the overall normalization of the galaxy population’s ionizing emissivity, i.e. the highly uncertain $\langle f_{\text{esc}}\xi_{\text{ion}} \rangle(z)$. In this manner, we have run a suite of simulations spanning a wide range of emissivity histories. In the ensuing discussion, we break these models up into three categories.

We begin with our fiducial models. The left and middle panels in the top row of Figure 1 show the reionization and emissivity histories, respectively, for a set of models that we calibrated to the Ly α forest mean transmission at $5 < z < 6$, as described in §2.1. The right panel compares the Ly α mean transmissions in the models to a collection of recent observational measurements. These models span a range of $\tau_{\text{es}} \in [0.047, 0.068]$, compatible with the most recent measurement of $\tau_{\text{es}} = 0.058 \pm 0.006$ based on Planck data [78]. We term these models FIDUCIAL-CALIBRATED.

In the next section, we will find that the starting epochs and cumulative ionizing photon outputs of the FIDUCIAL-CALIBRATED models scale with the kSZ power, suggesting that we may use existing limits on the power to draw broad conclusions about the high- z galaxy population. As a foil to these models, we have constructed a set of extreme scenarios. These are also calibrated to the forest transmission, but with emissivity histories designed to test the generality of the scaling relations. The middle row of Figure 1 shows our EXTREME-CALIBRATED models. The main features that result in our labeling these models “extreme” are the rapidity of the emissivity evolutions and their non-monotonic nature. In these models, the time-scale for the evolution, $t_{\text{em}} = \dot{N}_{\text{ion}} \left(\frac{d\dot{N}_{\text{ion}}}{dt} \right)^{-1}$, is at times much shorter than ($< 1/10$ th) the Hubble time. In contrast, the FIDUCIAL-CALIBRATED models have $t_{\text{em}} = \dot{N}_{\text{ion}} \left(\frac{d\dot{N}_{\text{ion}}}{dt} \right)^{-1} \sim H(z)^{-1}$ at all times before $z = 6$.⁴ These models nonetheless latch on to the forest constraints at $z < 6$ by construction and have CMB optical depths spanning $\tau \in [0.048, 0.073]$. We emphasize that the EXTREME-CALIBRATED models are illustrative in nature, and are not intended to represent physically plausible reionization scenarios.

Lastly, we consider another set of illustrative UNCALIBRATED models, shown in the bottom row, that are not calibrated to the forest constraints. As the bottom-left and bottom-right panels of Figure 1 show, reionization ends significantly earlier in these models than the forest constraints allow. This also results in some fairly high CMB optical depths spanning $\tau_{\text{es}} \in [0.051, 0.119]$. The purpose of the UNCALIBRATED models is to show how the forest constraints, when combined with the kSZ power, can be used to sharpen our view of reionization’s early phases.

3.2 Results

3.2.1 The Starting Epoch of Reionization

The first of our main results is displayed in Fig. 2, where we show the pkSZ power versus the starting epoch of reionization, z_{05} , defined here as the redshift at which the volume-average ionized fraction reaches 5%. The data points correspond to our models, with different

⁴This discussion pertains to $z > 6$, before the abrupt drop in ionizing emissivity seen at $z \lesssim 6$, which has been noted by several other authors (see e.g. Ref. [60] and references therein). The origin of this drop is still a matter of debate, which we do not take up here. We note that the contribution to the pkSZ power below $z = 6$ is small.

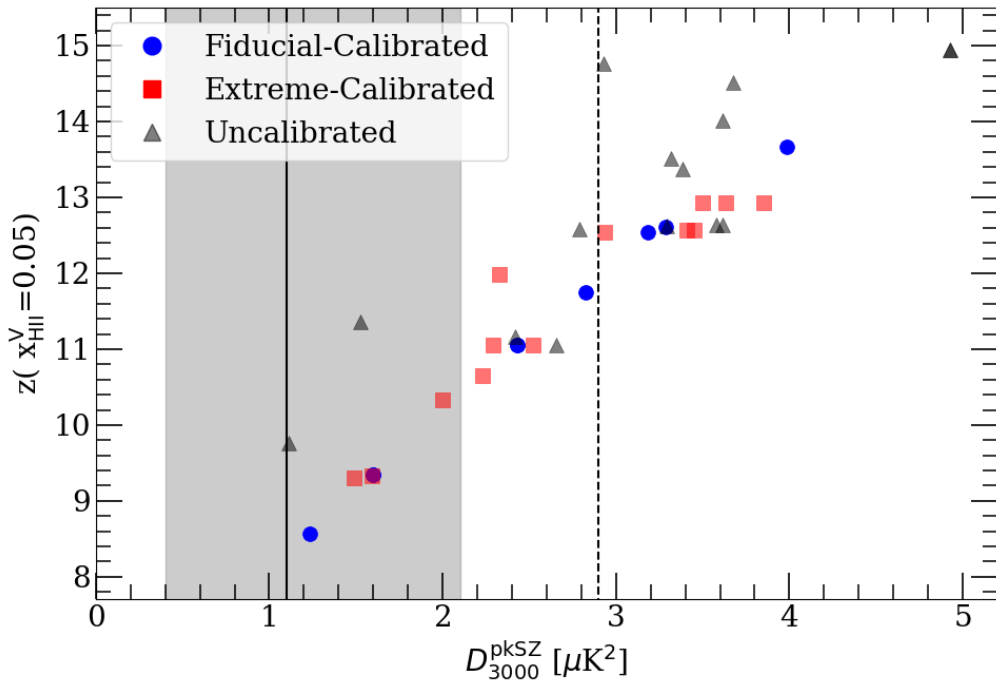


Figure 2. Correlation between patchy kSZ power at $\ell = 3000$ and the starting epoch of reionization (defined to be the redshift at which $x_{\text{HII}}^V = 5\%$). All models shown here adopt the same model for the clustering of ionizing sources. The FIDUCIAL-CALIBRATED models (blue circles) exhibit the tightest correlation between D_{3000}^{pkSZ} and z_{05} , but the correlation is still apparent for our other models. These results demonstrate that fixing the end of reionization, in accordance with Ly α forest constraints, makes the pkSZ power a probe of the starting epoch of reionization. In §4, we explore the effects of varying the source clustering model.

plot symbols denoting the categories introduced in the last section. For reference, the solid line, gray shaded region and black dashed line correspond to the measurement, 1- σ error bars and 95% confidence upper limit of Ref. [75], respectively. There is a tight correlation between D_{3000}^{pkSZ} and z_{05} , especially among the FIDUCIAL-CALIBRATED models (blue circles), noting again that all of the models in this section adopt effectively the same source clustering model. Qualitatively, the existence of a tight correlation is not sensitive to our choice for the ionized fraction threshold defining the starting epoch. The origin of this correlation can be understood as follows. Previous studies have highlighted the dependence of the pkSZ power on reionization’s duration and midpoint [74, 79–82], although see Refs. [71, 83, 84] and §5 for nuances. For most of our models, the end of reionization is tightly constrained by the Ly α mean transmission. While there is some variation among our models in the midpoint, most lie within the range permitted by CMB τ_{es} measurements. With the endpoint and midpoint of reionization being roughly fixed in most of our models, and the source clustering being fixed, it follows that D_{3000}^{pkSZ} scales with the starting epoch.

It is perhaps surprising that the EXTREME-CALIBRATED models do not exhibit more scatter in the relationship between z_{05} and D_{3000} , raising the broader question of why the correlation is so tight for the calibrated models. It is instructive to consider the conditions that give rise to the most extreme outlier, the UNCALIBRATED model denoted by the triangle

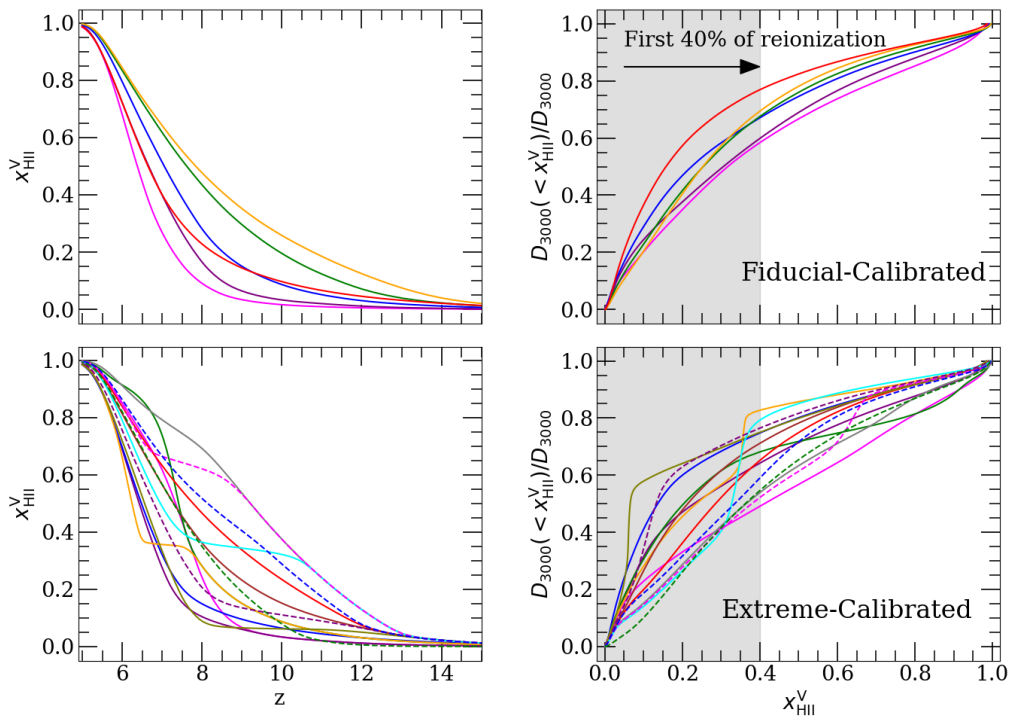


Figure 3. The accumulation of pkSZ power as a function of the global ionized fraction. The right panels show the fraction of D_{3000} accumulated before $x_{\text{HII}}^{\text{V}}$, while the left panels show the corresponding reionization histories for reference. The top and bottom rows show our FIDUCIAL-CALIBRATED and EXTREME-CALIBRATED models, respectively. For all of these models, 50-85% of D_{3000} comes from the earlier phases of reionization, $x_{\text{HII}} \leq 40\%$, which we illustrate with the shaded gray region.

at $D_{3000} \approx 3 \mu\text{K}^2$, $z_{05}=14.8$. The reionization history is quick and early in this model, with $x_{\text{HII}}^{\text{V}} = 1\%$ and 99% at $z \approx 15.1$ and 11.3 , respectively – a time span of just 130 Myr. The reionization history corresponds to the right-most olive curve in the bottom-left panel of Fig. 1.⁵ This scenario is not only un-physical in how quickly the ionizing emissivity rises; it also badly violates the Ly α forest constraints for the end of reionization. More broadly, for a fixed z_{05} , we find that it is difficult to construct a model with a much smaller D_{3000} that scatters far to the left, i.e. significantly above the relation, without violating the Ly α forest constraints imposed at $z \lesssim 6$.

What about scattering below the relation? Again, we find that it is generally difficult to construct models that increase the pkSZ power at a fixed z_{05} . To help understand why, in Fig. 3 we plot the fraction of D_{3000}^{pkSZ} accumulated at times before a global ionized fraction of $x_{\text{HII}}^{\text{V}}$ (right panels). For reference, the corresponding reionization histories are shown in the left panels. The top and bottom panels correspond to our FIDUCIAL-CALIBRATED and EXTREME-CALIBRATED models, respectively. These panels show that D_{3000} receives most (50-85%) of its contribution from the earlier phases of reionization, $x_{\text{HII}}^{\text{V}} < 40\%$. To construct

⁵Note that this model has a large pkSZ power in spite of its short duration because of our convention that all contributions from $z \geq 5.0$ are included in our definition of the pkSZ signal. We emphasize, however, that the existence of the tight correlation in Fig. 2 does not depend on this definition; the FIDUCIAL-CALIBRATED and EXTREME-CALIBRATED models are constructed to end near $z = 5 - 5.5$, so the changes in power are insignificant if we instead chose to place the demarcation between pkSZ and hKSZ at z_{99} .

a model that maximizes D_{3000} for fixed z_{05} (i.e. scatters significantly below the relation), features in the ionization fields with angular scale $\ell \sim 3000$, corresponding to $\theta \sim 0.06$ degrees, must be present for more of the light cone. To this end, we consider two models where the global ionized fraction lingers near $\sim 30\%$ for much of reionization’s duration. These are the two models in the bottom-right panel with sharp rises in D_{3000} at $x_{\text{HII}}^V \approx 30\%$. Even in these extreme scenarios, designed to pump up D_{3000} , we find that D_{3000} increases by a modest $\sim 15\%$. Again, further imposing conditions on the ionizing emissivity evolution based on physical grounds limits the scatter even more, as indicated by the blue circles in Figure 2.

From Fig. 2 we are led to several broad conclusions that apply for a fixed source clustering model. Reionization models that are calibrated to the Ly α forest mean transmission measurements at $z \lesssim 6$ generally exhibit a correlation between D_{3000}^{pkSZ} and the starting epoch of reionization, quantified here with z_{05} . This matches expectations from the literature, with the notable exception of Ref. [71], which found D_{3000} was not sensitive to z_{05} . We discuss this discrepancy more in §5. The correlation we find is tighter if the models are restricted to those with physically reasonable ionizing emissivity histories, i.e. monotonically rising at a rate of order the Hubble time, as in our FIDUCIAL-CALIBRATED models. Based on these findings, Figure 2 indicates that the existing 95% upper-limit on the pkSZ power reported by SPT [75] implies a corresponding rough upper limit of $z_{05} \lesssim 12$ for our $\dot{n}_{\text{ion}} \propto L_{\text{UV}}$ model. For the ACT measurement of Ref. [50], we adopt a conservative (low) estimate for the hkSZ contribution of $0.85 \mu\text{K}^2$, based on Ref. [49], to obtain an approximate 2σ upper limit of $D_{3000}^{\text{pkSZ}} \lesssim 2.05 \mu\text{K}^2$. This translates to $z_{05} \lesssim 11$ for the ACT measurement. These results are consistent with z_{05} values implied by constraints on the mid-point and duration of reionization in other works using the pkSZ [80, 81, 85].

Figure 2 highlights how the sharpening of pkSZ measurements by current and forthcoming CMB surveys, when combined with Ly α forest measurements, could place more stringent limits on the starting epoch of reionization. We emphasize that different assumptions about the source clustering will in general add variations to the pkSZ power for a fixed reionization history, a topic we explore in §4. Before addressing that, we turn to the ionizing photon output of the galaxy population.

3.2.2 Ionizing Photon Production of Early Galaxies

The starting epoch of reionization is set by the ionizing photon output of the high- z galaxy population. We now explore what the pkSZ power can tell us about this output. We quantify it with the the cumulative number of ionizing photons emitted into the IGM per hydrogen atom up to a cosmic time t_* :

$$N_{\gamma/H}(z \geq z_*) = \int_{t_0}^{t_*} \frac{\dot{n}_{\text{ion}}(t)}{n_{\text{H}}(t)} dt, \quad (3.1)$$

where \dot{n}_{ion} is the global rate of ionizing photon emission per unit volume, n_{H} is the cosmic mean hydrogen density, and z_* is the redshift at the reference time t_* . In what follows, we will use the notation $N_{\gamma/H}^{z_*} \equiv N_{\gamma/H}(z \geq z_*)$. We begin the integration at $z = 18$, consistent with the start of our RT simulations.

In Figure 4 we plot $N_{\gamma/H}^{z_*}$ versus D_{3000} for $z_* = 8$ and $z_* = 12$ in the left and right panels, respectively. For reference, the cosmic time interval between these redshifts is ≈ 270 Myr. Again, the solid black line, shaded gray region and dashed line denote the mean value, $1\text{-}\sigma$ error bars and 95% confidence upper limits of the SPT measurement [75]. A key result

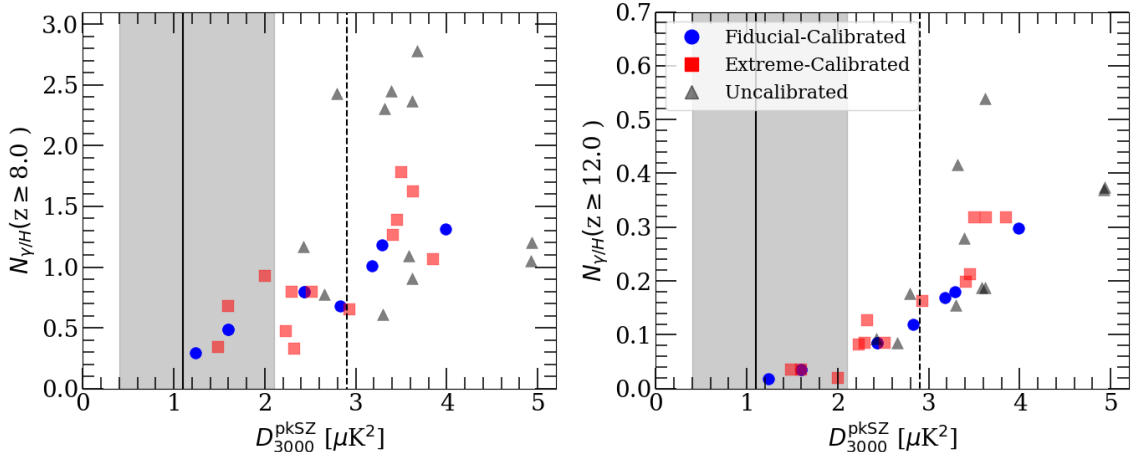


Figure 4. Correlation of the ionizing photon budget of the galaxy population with the pkSZ power given Ly α forest constraints on the end of reionization. The left and right panels show the cumulative number of ionizing photons emitted into the IGM per hydrogen atom before a redshift of $z_* = 8$ and $z_* = 12$, respectively (see eq. 3.1) as a function of pkSZ power. In both panels, there is a prominent trend between the $N_{\gamma/H}^{z_*}$ and D_{3000} , especially for the FIDUCIAL-CALIBRATED models. Existing D_{3000} measurements can place model-dependent upper bounds on the ionizing photon outputs of early galaxies.

here is the correlation between D_{3000} and $N_{\gamma/H}^{z_*}$ in the FIDUCIAL-CALIBRATED models (blue-circles). This result is a consequence of the $z_{05} - D_{3000}$ correlation discussed in the previous section, and the fact that the reionization history is set by the ionizing photon production of the sources minus the absorption rate by the sinks. Note that there is significantly less scatter in the $N_{\gamma/H}^{12} - D_{3000}$ relation (right panel), compared to the $N_{\gamma/H}^8 - D_{3000}$ relation (left panel) – particularly for $D_{3000} \lesssim 3.0 \mu\text{K}^2$. Appealing to Figure 2, we can see that models with $D_{3000} \lesssim 3.0 \mu\text{K}^2$ should have $z_{05} \lesssim 13$. Hence, any variation in $N_{\gamma/H}^{12}$ for fixed D_{3000} must arise from variations in the reionization history within a quite narrow window range in cosmic time, which reduces the scatter among these models.

Figure 4 suggests that we can estimate a rough upper limit on the ionizing photon production of early galaxies in our models. The 95% upper SPT limit on D_{3000} translates to a limit of $N_{\gamma/H} \lesssim 1.0$ ionizing photon produced per hydrogen at $z > 8$ for our $\dot{n}_{\text{ion}} \propto L_{\text{UV}}$ source model. This becomes $N_{\gamma/H} \lesssim 0.15$ for $z > 12$. Regarding the ACT measurement, if we again assume a value of $0.85 \mu\text{K}^2$ for the hkSZ contribution, the lower D_{3000} reported by them tightens these limits to $N_{\gamma/H} \lesssim 0.7$ and 0.08 for $z \geq 8$ and 12 , respectively. (All estimates here do not include our EXTREME and UNCALIBRATED models.) It is interesting to compare these estimates to the models in Ref. [34], which were mentioned in the introduction to this paper. In their fiducial “photon budget crisis” model, the observed galaxy population emits ≈ 1.6 photons per hydrogen atom into the IGM before $z = 8$. This number increases to ≈ 3.1 if the UV luminosity function is extrapolated down to $M_{\text{UV}} = -13$.

The results in this section, which are restricted to a single emissivity-halo prescription, have served mainly to illustrate the relationships between the reionization history, ionizing emissivity, and pkSZ power, and to build intuition for them. We now turn to the important effect that source clustering has on these relationships.

4 Effect of Source Clustering on pkSZ Power

4.1 Quantifying the Effect of Source Clustering

In this section, we investigate how the pkSZ power depends on the assumed model of source clustering. As discussed in the introduction, the faint end of the UV luminosity function during reionization remains highly uncertain. Moreover, there is no broad consensus on the ionizing photon production efficiencies and escape fractions of even the observed high- z galaxies. As such, we adopt 3 emissivity-halo prescriptions that are designed to bracket a wide range of source clustering possibilities:

- $\dot{n}_{\text{ion}} \propto L_{\text{UV}}$ – This is the same model used in previous sections. Recall that all halos more massive than $10^9 h^{-1} M_{\odot}$ are sources of ionizing photons. The rate of ionizing photon emission into the IGM is assumed proportional to UV luminosity.
- UV-BRIGHT – This model also assumes the proportionality $\dot{n}_{\text{ion}} \propto L_{\text{UV}}$, but implements a cutoff such that only galaxies brighter than $M_{\text{UV}} = -18$ contribute. This is a scenario in which the brightest observed galaxies are the sole drivers of reionization (see e.g. [86, 87] for empirical arguments in favor of related scenarios).
- DEMOCRATIC – In this model, all galaxies emit ionizing photons at the same rate, independent of UV luminosity ($\dot{n}_{\text{ion}} \propto \text{const}$). Effectively, this represents a scenario in which the ionizing photon budget is dominated by the faintest (and therefore undetected) galaxies, owing to their abundance.

In the standard picture of hierarchical galaxy formation, it is generally assumed that scenarios like our UV-BRIGHT model would result in a more delayed and perhaps rapid reionization process, compared e.g. to the DEMOCRATIC model. This assumption is rooted in the fact that the most massive galaxies, on average, form later in the cosmological timeline. But given the large uncertainties in the ionizing photon outputs of galaxies, here we attempt to decouple the effects of source clustering from the reionization history. This allows us to isolate the effects of source clustering/morphology on the pkSZ power. We note that this approach is different from many previous discussions of source clustering/morphology in the pkSZ literature [e.g. 71, 79, 81, 83], which do not attempt to isolate those effects from differences in the reionization history (but see [80, 88] for studies that do).

To this end, we select a few representative FIDUCIAL-CALIBRATED reionization histories from the models of the last section, which adopt the $\dot{n}_{\text{ion}} \propto L_{\text{UV}}$ emissivity-halo prescription. We run two variations of each model using the UV-BRIGHT and DEMOCRATIC emissivity-halo prescriptions. Importantly, we do not change the input emissivity histories for these variations. This results in small changes in the early global reionization history, $\Delta x_{\text{HII}} \sim 0.01$ at $z \sim 8-10$, and somewhat larger changes later, $\Delta x_{\text{HII}} \sim 0.05$ at $z \sim 5.5-6.5$. We note that these small changes should not significantly affect our results, as the majority of the D_{3000} contributions come from early times, as shown above. The variation in the source clustering has a larger impact on the pkSZ power through changes in the morphology of ionized regions – the effect that we focus on in this section.⁶

⁶With this procedure, we also find that the calibration to the Ly α forest mean transmission fraction is mostly preserved; the deviations are again largest at $z \sim 6$, where they vary by $\sim 50\%$. We do not recalibrate the models, as doing so would not significantly change D_{3000} .

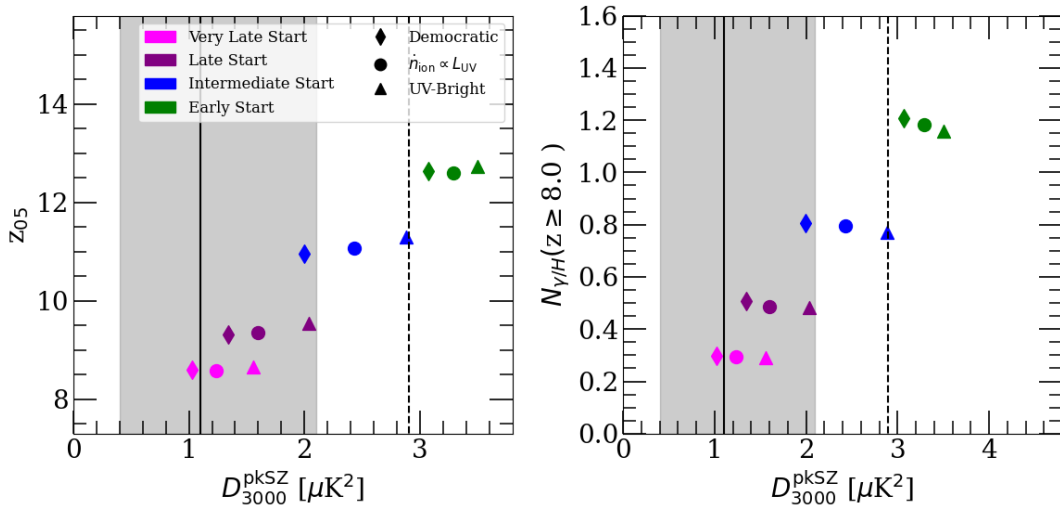


Figure 5. The effect of source clustering/reionization morphology on the pkSZ power. The left and right panels show the $D_{3000} - z_{05}$ and $D_{3000} - N_{\gamma/H}^8$ relationships, respectively. Colors correspond to different reionization histories, while marker styles correspond to different emissivity-halo prescriptions. For a fixed color, the range in D_{3000}^{pkSZ} values quantifies how much the pkSZ power varies under our different source prescriptions for a fixed reionization history. Models with more biased ionizing sources exhibit more large-scale power in the ionization field which, in turn, leads to more pkSZ power.

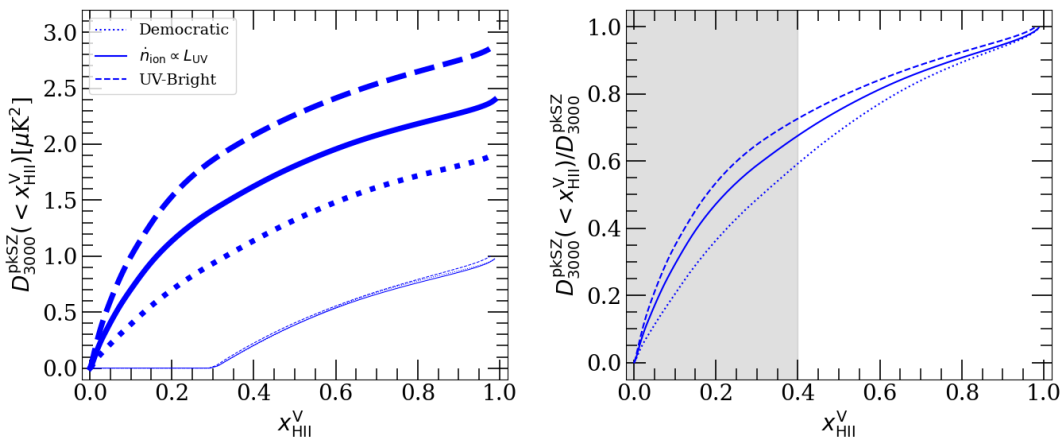


Figure 6. Source clustering imprints differences in the pkSZ power within the first 30% of reionization. *Left:* The accumulation of D_{3000}^{pkSZ} as a function of $x_{\text{HII}}^{\text{V}}$ compared among our emissivity-halo prescriptions for the fixed INTERMEDIATE START reionization history (same as the blue points in Fig. 5). Thick curves show the accumulation over the entire reionization history, whereas the thin curves show only the growth in D_{3000}^{pkSZ} over the last 70% of reionization. *Right:* The fraction of D_{3000}^{pkSZ} accumulated by an ionized fraction of $x_{\text{HII}}^{\text{V}}$ for the same model set. For a fixed reionization history, the fraction of power that originates from $x_{\text{HII}}^{\text{V}} \lesssim 40\%$ scales with the clustering strength of the sources.

Figure 5 quantifies the variations in D_{3000}^{pkSZ} that arise from our different source clustering prescriptions. We show both z_{05} vs D_{3000}^{pkSZ} (left panel) and $N_{\gamma/H}^8$ vs D_{3000}^{pkSZ} (right panel).

The different colors denote different reionization histories, as labeled qualitatively in the plot legend according to when reionization starts. The circles, triangles, and diamonds correspond to the $\dot{n}_{\text{ion}} \propto L_{\text{UV}}$, UV-BRIGHT, and DEMOCRATIC emissivity-halo prescriptions, respectively. Note, for a given reionization time line (e.g. the INTERMEDIATE START models), the fact that z_{05} and $N_{\gamma/H}^8$ stay approximately constant between the different source prescriptions indicates that the three reionization histories are approximately the same, as already noted above. (The small variations in $N_{\gamma/H}^8$ seen in the right panel owe to small inaccuracies in our RSLA correction. Although we hold the $\tilde{c}/c = 0.2$ emissivities fixed, applying the RSLA correction for simulations with different source models can produce slightly different $\tilde{c}/c = 1$ results – see Eq. 2.1.) The corresponding range in the D_{3000}^{pkSZ} values quantifies how much the pkSZ power can vary under different source prescriptions for a fixed reionization history. For example, for the INTERMEDIATE START models, D_{3000}^{pkSZ} varies between $1.98 \mu\text{K}^2$ for the DEMOCRATIC model to $2.88 \mu\text{K}^2$ for the UV-BRIGHT model. Indeed, we find variations of 35-50% owing to source clustering alone across the different models.⁷ Intuitively, models with more biased ionizing sources exhibit more large-scale power in the ionization field in the first \sim third of reionization which, in turn, leads to more pkSZ power for a fixed reionization history.

Figure 6 considers the question of where these differences arise. There we compare emissivity-halo prescriptions for a fixed reionization history (INTERMEDIATE START). Similar to Figure 3, the right panel shows the fraction of D_{3000}^{pkSZ} accumulated before a time corresponding to $x_{\text{HII}}^{\text{V}}$. In the left panel, the thick/top set of curves show the absolute $D_{3000}^{\text{pkSZ}} (< x_{\text{HII}}^{\text{V}})$ over the entire reionization history, while the thin/bottom set of curves start the accumulation at $x_{\text{HII}}^{\text{V}} = 30\%$. The results in the left panel make clear that the differences in D_{3000}^{pkSZ} across source models occurs almost exclusively at early times, $x_{\text{HII}}^{\text{V}} \lesssim 30\%$. In fact, for the reionization histories considered in this section, we find that the relative difference in power originating from the last $\sim 70\%$ of reionization is $\lesssim 5\%$ across source models.⁸

We emphasize that the results in this section should be taken as a rough upper limit on the effect of source clustering, for a fixed reionization history. If the source clustering is connected to the reionization history in the way usually assumed, it would decrease the spread in D_{3000}^{pkSZ} values. For example, if reionization is delayed in our UV-BRIGHT model (because we have to wait for more massive halos to form), this would have the effect of decreasing D_{3000}^{pkSZ} , therefore bringing it closer to the $\dot{n}_{\text{ion}} \propto L_{\text{UV}}$ result. Likewise, D_{3000}^{pkSZ} would move upward in our DEMOCRATIC model if reionization starts earlier in that scenario. We will discuss scenarios with evolving emissivity-halo prescriptions in §5.1.

4.2 Breaking the Degeneracy with Source Clustering

The results in Figure 5 show how uncertainties in the sources of reionization complicate the connection between D_{3000}^{pkSZ} and the ionizing output of high- z galaxies. The issue is that the effect of reionization’s morphology on D_{3000}^{pkSZ} (as set by the source clustering) is degenerate with the reionization history. In this section, we explore the possibility of breaking this degeneracy with additional information. Section 4.2.1 considers the usage of the $z = 5 - 6$ Ly α forest opacity fluctuations, while Section 4.2.2 considers the use of the shape of the pkSZ spectrum.

⁷This is a larger spread than seen by Ref. [80], but consistent with Refs. [51, 88]. Our models likely bracket a much wider range of reionization morphologies than in Ref. [80], which may account for the difference.

⁸In absolute terms, this reflects a typical difference of $\sim 0.05 \mu\text{K}^2$, but goes up to $\sim 0.1 \mu\text{K}^2$ for our EARLY

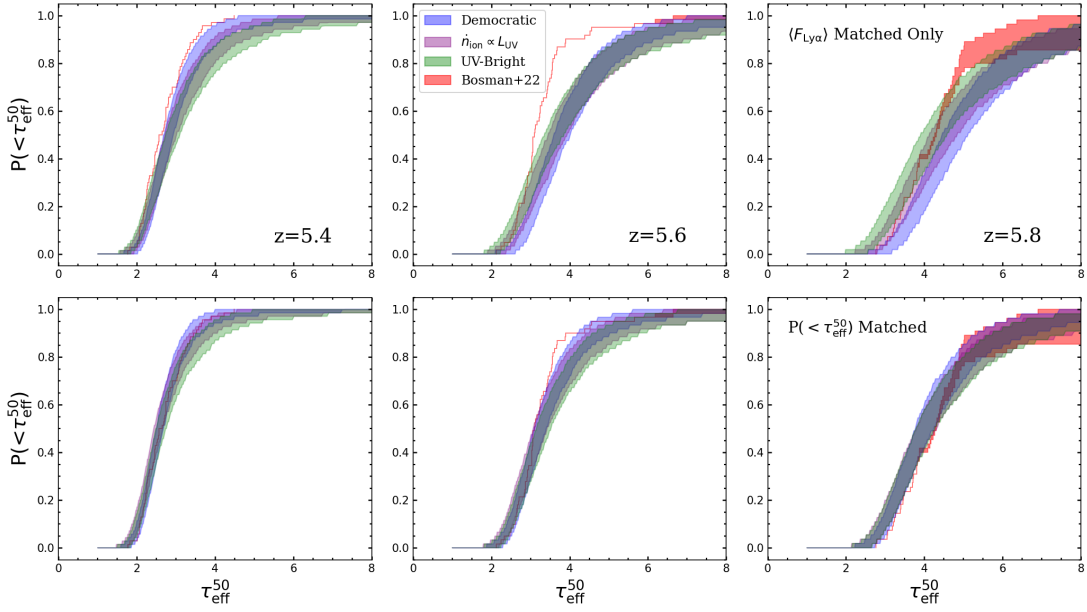


Figure 7. Adjusting the calibration of our models for agreement with the observed Ly α forest opacity fluctuations. The panels show the cumulative probability distribution function of the Ly α forest effective optical depth, τ_{eff} . The red histograms show observational measurements from Ref. [15]. The other colors correspond to different emissivity-halo prescriptions for a fixed reionization history (LATE START; purple data points in Fig. 5). The top row shows distributions from our original models, which are calibrated only to the mean transmission fraction, $\langle F_{\text{Ly}\alpha} \rangle$. Despite this calibration, the models generally do not agree well with the observed distributions. The bottom row shows the models after they have been recalibrated to the observed distributions. The left panel of Figure 8 shows how the reionization histories were perturbed to achieve these recalibrations.

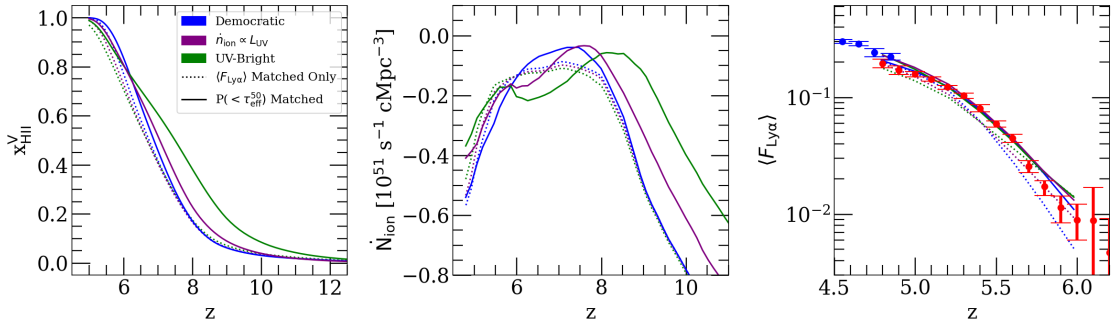


Figure 8. Recalibrating our models for agreement with the Ly α forest opacity fluctuations. The left, middle, and right panels show the reionization histories, emissivity histories, and Ly α forest mean transmission fractions in our LATE START models. As in Figure 7, colors denote different emissivity-halo prescriptions. The dotted curves show the original models, which are calibrated to only the mean transmission fraction, while the solid curves show the models after recalibrating to $P(< \tau_{\text{eff}}^{50})$.

START model.

4.2.1 The Ly α Forest Opacity Fluctuations

The models discussed in the previous sections were calibrated to match the observed mean transmission of the Ly α forest. This calibration, however, does not guarantee agreement with the observed opacity fluctuations at $5 < z < 6$. In fact, we find that our calibrated models in which the sources are more clustered tend to over-predict the fluctuation amplitude. We illustrate this in the top row of Figure 7 using our LATE START models (purple data points in Figure 5). All panels show $P(< \tau_{\text{eff}}^{50})$, the cumulative probability distribution function of the effective optical depth, τ_{eff}^{50} . Here, $\tau_{\text{eff}}^{50} \equiv -\ln\langle F_{\text{Ly}\alpha} \rangle_{50}$, where the average is over a pathlength of $50 h^{-1}\text{cMpc}$, and $F_{\text{Ly}\alpha}$ is the continuum-normalized flux, i.e. the transmission fraction. The left, middle, and right panels correspond to $z = 5.4, 5.6,$ and 5.8 , respectively. The red histograms show the observational measurements of Ref. [15], while the other shaded regions correspond to the 10th and 90th percentiles obtained by bootstrap resampling $P(< \tau_{\text{eff}}^{50})$ in the different source clustering models, as indicated in the legend. Across redshift, the $P(< \tau_{\text{eff}}^{50})$ is too wide in all of the models, indicating an overall excess in τ_{eff}^{50} fluctuations for the LATE START scenarios. This excess is caused by there being too many neutral islands in the $z < 6$ IGM in the LATE START models.

A key point here is that, for a fixed source clustering model, achieving better agreement with the observed width of $P(< \tau_{\text{eff}}^{50})$ requires perturbing the reionization history to reduce the global neutral fraction at $z < 6$. We illustrate this in the bottom row of Figure 7. There, we consider the same source clustering models, but we have perturbed the LATE START reionization histories to achieve better agreement with the observed width of $P(< \tau_{\text{eff}}^{50})$, while also maintaining good agreement with the mean transmission fraction. The new reionization histories are shown as the solid curves in the left panel of Figure 8, against the original histories (dashed curves). Note that the original histories are very close to each other by design because they were used in the previous section to isolate the effects of source clustering.

For the $\dot{n}_{\text{ion}} \propto L_{\text{UV}}$ and UV-BRIGHT source models, the narrowness of the observed $P(< \tau_{\text{eff}}^{50})$ favors histories in which reionization begins somewhat earlier. The reason is that perturbing the end of reionization to reduce the neutral fraction at $z < 6$ results in too much overall transmission in the forest, overshooting the observed $\langle F_{\text{Ly}\alpha} \rangle$ evolution. This problem is amplified in models with larger fluctuations in the ionizing background owing to the enhanced forest transmission near the sources. Indeed, among our three models, the UV-BRIGHT source model overshoots $\langle F_{\text{Ly}\alpha} \rangle$ the most when the neutral fraction is reduced at $z < 6$. We find that further perturbing the reionization history to start earlier allows us keep the neutral fraction sufficiently low to match the width of $P(< \tau_{\text{eff}}^{50})$, while at the same time maintaining reasonable agreement with the $\langle F_{\text{Ly}\alpha} \rangle$ evolution. This occurs because the mean photo-ionization rate in the ionized IGM can afford to be lower at $z < 6$ if a larger fraction of reionization took place early. These points are illustrated in Figure 8. Note that the fluctuation amplitude of the ionizing background is significantly lower in the DEMOCRATIC source model. Hence, reducing the neutral fraction at $z < 6$ does not result in such a sharp increase in $\langle F_{\text{Ly}\alpha} \rangle$. In fact, for the illustrative example in Figure 8, we do not find the need to perturb the earlier phase of reionization in the DEMOCRATIC model.

In Figure 9, we illustrate how these re-calibrations to include the $P(< \tau_{\text{eff}}^{50})$ constraints affect the relationships between D_{3000}^{pkSZ} , z_{05} , and $N_{\gamma/H}^8$. Here, we include a re-calibrated set of EARLY reionization models (not shown in Figure 8; see the green points in Figure 5). The re-calibrated LATE and EARLY models are shown as purple and red points respectively. The different plot symbols correspond to the variation of source clustering model, as indicated

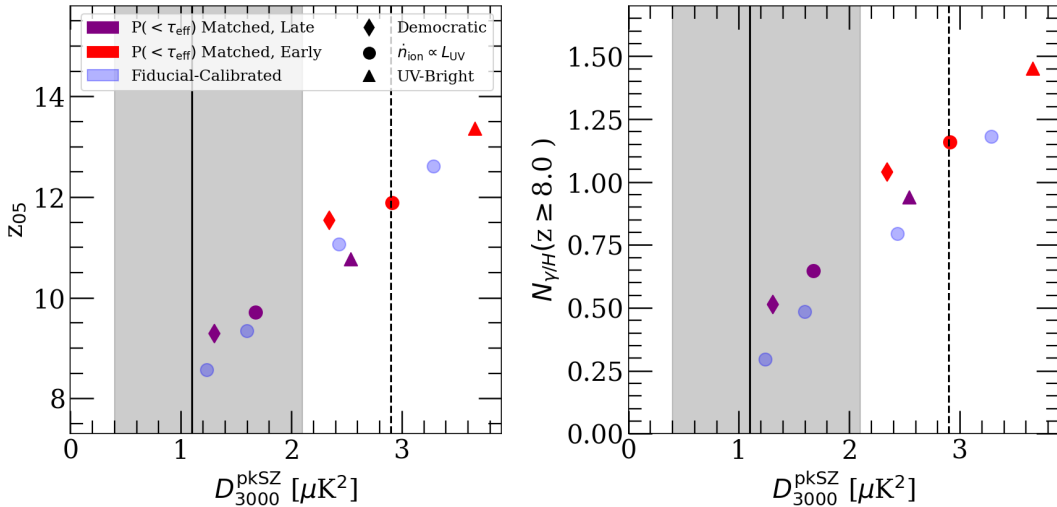


Figure 9. The same as Figure 5, but for models re-calibrated to improve agreement with the Ly α forest opacity fluctuations. The purple and red points correspond to the LATE and EARLY reionization histories, while the plot markers denote different emissivity-halo prescriptions. For reference, the light blue circles show a selection of the FIDUCIAL-CALIBRATED models from §3, illustrating the sharp correlations found in that section. The alterations to the reionization histories driven by the recalibrations (see Fig. 8) tend to push models more in line with the FIDUCIAL-CALIBRATED models. These results show that including the observed Ly α forest opacity fluctuations among the constraints on the end of reionization helps break the degeneracy in D_{3000}^{pkSZ} between the early reionization history and source clustering.

in the legend. For reference, the light blue circles show a sub-sample of the FIDUCIAL-CALIBRATED models (with $\dot{n}_{\text{ion}} \propto L_{\text{UV}}$) discussed in §3. These points are reproduced here to show the trends discussed previously.

In Figure 5, we saw that changing the source clustering for fixed reionization history modulated D_{3000}^{pkSZ} while preserving z_{05} and $N_{\gamma/H}^8$, spoiling the tight scalings discussed in §3. Here, we find that including the $P(< \tau_{\text{eff}}^{50})$ constraints perturbs the reionization history in a way that somewhat recovers the previously noted scalings between pkSZ power, z_{05} , and $N_{\gamma/H}^8$. Comparing directly to Figure 5, we see that the $\dot{n}_{\text{ion}} \propto L_{\text{UV}}$ and UV-BRIGHT models – especially the latter – move upward and to the right, i.e. increasing in D_{3000}^{pkSZ} , z_{05} , and $N_{\gamma/H}^8$, for the reasons described above. This recovers somewhat the tight scaling relations found in Figure 2. We caution that the particular models shown here are merely illustrative. They nonetheless serve to highlight how including the τ_{eff} fluctuation amplitude in the empirical constraints can help break the D_{3000}^{pkSZ} degeneracy between reionization history and morphology.

4.2.2 The Shape of the pkSZ Power Spectrum

Another potential way forward is to consider the pkSZ power spectra at additional scales. Observationally, this has proved challenging due to primary CMB anisotropies increasingly dominating at $\ell \lesssim 3000$ and foregrounds dominating at $\ell \gtrsim 3000$. However, given recent developments in foreground mitigation methods, Ref. [51] forecast the ability to isolate the pkSZ signal on scales $\ell \in [2500, 5000]$ in the near future. Measurements at these additional

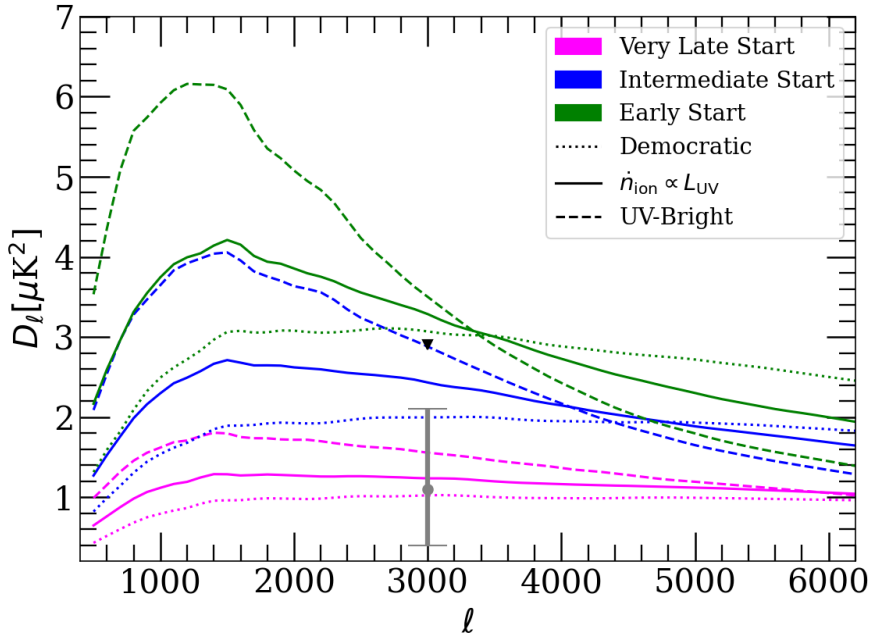


Figure 10. The interplay between reionization history and morphology in shaping the pkSZ angular power spectrum. The colors denote different reionization histories, while the line styles denote different emissivity-halo prescriptions. The DEMOCRATIC source models (least biased sources) have much flatter power spectra. Conversely, the UV-BRIGHT models (highly biased sources) have the steepest slope. These results suggest that the degeneracy between reionization history and source clustering can be mitigated by examining the slope and amplitude of pkSZ power spectrum.

scales could give us crucial information on the clustering of ionizing sources, the utility of which we explore in this section.

To start, we plot the pkSZ angular power spectrum, D_ℓ^{pkSZ} , in Figure 10 for several combinations of source models and reionization histories. DEMOCRATIC, $\dot{n}_{\text{ion}} \propto L_{\text{UV}}$, and UV-BRIGHT prescriptions are represented by dotted, solid and dashed lines, respectively, with different colors denoting different reionization histories according to the legend. It is apparent that both the slope and amplitude of D_ℓ^{pkSZ} around $\ell = 3000$ are dependent on the source clustering, with the DEMOCRATIC models having flat slopes, and the UV-BRIGHT models having the steepest slopes. These differences arise from the different morphologies of ionized regions between source models. At fixed ionized fraction, UV-BRIGHT models have the largest ionized bubbles on average, so they generate more pkSZ power on larger scales (lower ℓ), compared to the other source models. A complication, however, is that longer reionization histories strengthen the impact of morphology on the D_ℓ^{pkSZ} slope. This is the most noticeable among the UV-BRIGHT models (dashed curves). Intuitively, extending the reionization history means that CMB photons pass through more ionized structures which imprint more temperature anisotropies, increasing the overall amplitude of D_ℓ^{pkSZ} . However, for different reionization morphologies, the pkSZ power at different scales will increase by different amounts, altering the D_ℓ^{pkSZ} slope in a morphology-dependent way. This intuition suggests that the history-source degeneracy can be mitigated by examining the slope and amplitude of D_ℓ^{pkSZ} simultaneously.

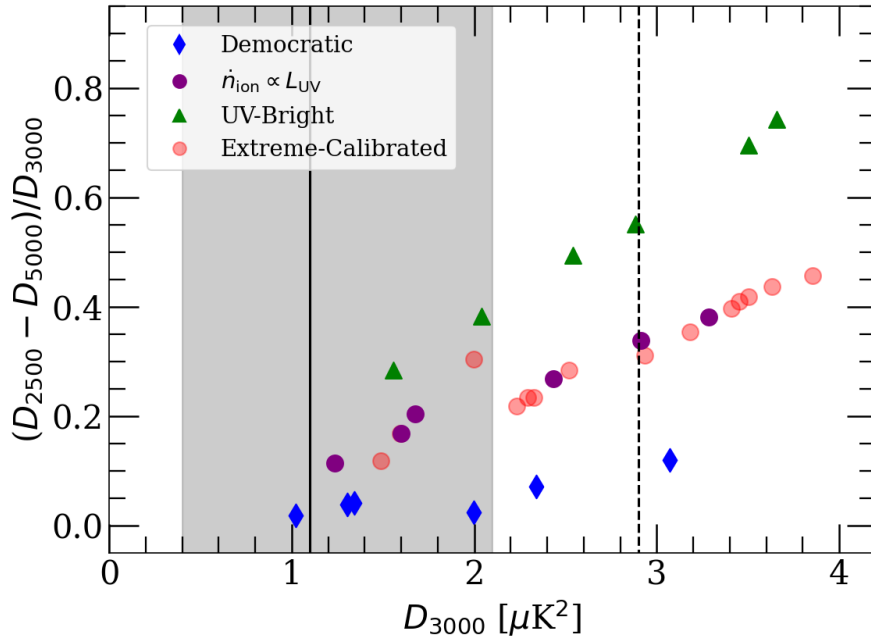


Figure 11. Relationship between the slope of the pkSZ power spectrum and its amplitude around $\ell = 3,000$ for a set of models spanning a wide range of reionization histories and source clustering prescriptions. (See main text for details.) On the ordinate, the slope over $2500 \leq \ell \leq 5000$ is normalized by the value D_{3000} . Different source clustering prescriptions segregate into different trends as indicated by the marker styles. If future CMB experiments are able to measure the pkSZ power at multiple angular scales, then the slope of the power spectrum can help break the degeneracy between reionization history and source clustering, especially if D_{3000} turns out to be on the high side of the values allowed by existing measurements.

In Figure 11, we plot the normalized power spectrum slope, defined here to be $(D_{2500} - D_{5000})/D_{3000}$, as a function of D_{3000} for a sample of models spanning different reionization histories and source clustering prescriptions.⁹ This visualizes how steep the slope is relative to the power amplitude. DEMOCRATIC, $\dot{n}_{\text{ion}} \propto L_{\text{UV}}$ and UV-BRIGHT prescriptions are represented by blue diamonds, purple circles and green triangles, respectively. We additionally include EXTREME-CALIBRATED models (with fixed $\dot{n}_{\text{ion}} \propto L_{\text{UV}}$ sources) as the faded red circles. The key result of Figure 11 is that different source prescriptions follow different trend lines. For example, DEMOCRATIC models fall quite low across the D_{3000} range, reflecting their flat D_ℓ slopes. In contrast, $\dot{n}_{\text{ion}} \propto L_{\text{UV}}$ and UV-BRIGHT models show distinct trends of steepening slopes with increasing D_{3000} , with the latter’s power spectra being around twice as steep as the former’s for the same D_{3000} . Reassuringly, these trends seem to hold across the range of histories considered, including both $P(< \tau_{\text{eff}}^{50})$ MATCHED models and even the majority of EXTREME-CALIBRATED models.¹⁰ If indeed future experiments are able to

⁹The ℓ values are selected to align with the range specified in the aforementioned forecasts of Ref. [51], but we do not expect our results to be sensitive to these choices.

¹⁰The notable exception in the EXTREME-CALIBRATED set at $(\sim 2\mu\text{K}^2, \sim 0.3)$ is a history where reionization starts with an extremely rapid growth in emissivity. In such a scenario, small ionized structures at very low $x_{\text{HII}}^{\text{V}}$ do not persist long and imprint less power at small scales, resulting in a steeper slope.

measure the pkSZ signal over $\ell \in [2500, 5000]$, then the slope of the power spectrum may help break the degeneracy between reionization history and source clustering. We note, however, that the usefulness of the slope is limited by the overall power amplitude; the differences in the slope increase with D_{3000} . Indeed, our results suggest that the slope may be of limited utility if D_{3000} turns out to be low, e.g. near the central value of the existing measurements by Refs. [47, 50].

5 Discussion

All of the models in our main results adopt a temporally fixed emissivity-halo relationship. For instance, in the $\dot{n}_{\text{ion}} \propto L_{\text{UV}}$ models, the emissivity assigned to each source is assumed proportional to its UV luminosity which, in turn, is mapped uniquely to a halo mass through abundance matching. In this sense, although the overall normalization of the emissivity evolves with time (owing to our calibration to the forest data), the emissivity-halo connection remains fixed. It is easy to imagine, however, that the emissivity-halo connection evolves during reionization. For example, smaller/fainter sources might start reionization before giving way to more massive galaxies as the former succumb to feedback processes [71, 89, 90]. There is also the issue of stochastic star formation, especially at the highest redshifts of interest. Recent observations provide evidence for extreme burstiness at these epochs [28, 91–97]. In §’s 5.1 and 5.2, we use illustrative models to argue that such effects are unlikely to change our broad conclusions. In §5.3, we compare the results discussed above to the findings of previous studies.

5.1 Models with evolving emissivity-halo connection

Consider a scenario in which reionization is started by smaller halos, but finished by more massive halos. We develop a simple ansatz to obtain a rough upper limit for how much this kind of evolving emissivity-halo connection would change our results. In the ansatz, the sources start out identical to our DEMOCRATIC model and evolve into the UV-BRIGHT model. To achieve this, we adopt the mapping $\dot{n}_{\text{ion}} \propto L_{\text{UV}}^\beta$ and assume that β evolves from 0 to 1 linearly in redshift. Additionally, the cutoff in UV-magnitude above which sources have zero emissivity, $M_{\text{UV}}^{\text{Cut}}$, evolves from -10 to -18 linearly over the same time interval. (Note that $\beta = 0$, $M_{\text{UV}}^{\text{Cut}} = -10$ and $\beta = 1$, $M_{\text{UV}}^{\text{Cut}} = -18$ correspond to our DEMOCRATIC and UV-BRIGHT models, respectively.) As shown in Figure 3, D_ℓ receives most of its contribution at $x_{\text{HII}} \lesssim 40\%$. Hence, we chose to vary these parameters quickly over $x_{\text{HII}} \sim 10\% - 35\%$, i.e. the transition from DEMOCRATIC to UV-BRIGHT occurs before $x_{\text{HII}} \sim 35\%$. This rapid evolution corresponds to timescales of $\sim 170 - 240$ Myr, for our shortest and longest FIDUCIAL-CALIBRATED histories, respectively. We emphasize that this extreme model is for illustrative purposes, and we use it here to gauge a rough upper limit for the effect.

Figure 12 considers the slope of the pkSZ power spectrum versus D_ℓ (as in Fig. 11), this time showing results from the models with evolving emissivity-halo connection as the purple squares. For comparison, the gray diamonds, circles and squares represent a selection of the DEMOCRATIC, $\dot{n}_{\text{ion}} \propto L_{\text{UV}}$, and UV-BRIGHT models from Figure 11. We see that the evolving models exhibit modestly steeper slopes than the DEMOCRATIC models, while preserving similar D_{3000} . Notably, despite the extremely quick evolution toward UV-BRIGHT (for the last $\sim 60\%$ of reionization, the sources are nearly identical to those in the UV-BRIGHT models), the evolving models present mostly like the DEMOCRATIC ones. A more realistic/slower evolution in the emissivity-halo connection would yield slopes even closer to

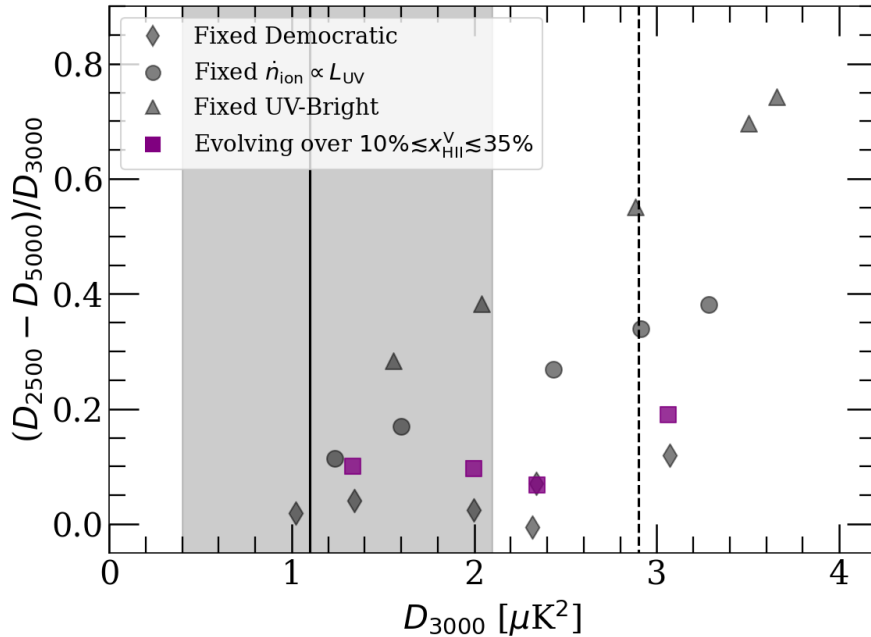


Figure 12. The same as Figure 11, but for models in which the emissivity-halo connection evolves in time. For reference, the gray data points reproduce some of the same models shown in Figure 11. The purple squares show new models where reionization begins with the DEMOCRATIC source prescription, but evolves into the UV-BRIGHT prescription during the interval $10\% \lesssim x_{\text{HII}}^V \lesssim 35\%$. This time scale is extremely rapid and chosen to maximize the change in D_ℓ for illustrative purposes. Even in this extreme case, we see that the evolving source models are only modestly different than the DEMOCRATIC models, with somewhat steeper slopes and similar amplitude. The takeaway is the slope of the pkSZ power around $\ell = 3,000$ appears to be most sensitive to the clustering of the sources that drive the first $\sim 30\%$ of reionization. Since the evolving models start out identical to the DEMOCRATIC models, they are most similar in this plot.

the DEMOCRATIC results. This finding supports the idea, raised in §3.2.1 and §4, that the pkSZ power spectrum probes the source properties during the first $\sim 30\%$ of reionization. The key takeaway from this section is that the slope of the pkSZ power around $\ell = 3,000$ appears to be most sensitive to the clustering of the sources that drive the first $\sim 30\%$ of reionization, consistent with §4. Any changes to the emissivity-halo connection that occur later have only a modest effect on the shape of the power spectrum.

5.2 Stochastic Star Formation

Stochastic star formation has been invoked to explain the abundance of UV-bright galaxies at $z > 10$ [18–26, 98–104]. Indeed, the spectral energy distributions of UV-bright galaxies at this epoch show evidence of ongoing starbursts [28, 91–97]. While we already use the UV luminosity functions derived from JWST observations, stochastic star formation histories can complicate the emissivity-halo connection in a way not captured by our abundance matching model. What if a significant fraction of the UV-bright galaxies in the observed UV luminosity function actually reside within low-mass halos that happen to be undergoing intense bursts of star formation, altering the effective clustering strength of the sources? In this section, we

use a simple model to test such a scenario.

The basic features of our simplistic approach are motivated by the semi-analytic model of Ref. [98]. Their model adopts a timescale of $\sim 5 - 30$ Myr between star formation and stellar feedback episodes. Star formation proceeds uninhibited over this time scale, resulting in a massive starburst. In smaller halos, the associated feedback is strong enough to drive gas out of the galaxy and quench star formation. For these halos, the model of Ref. [98] predicts a change in the rest-frame UV magnitude, M_{UV} , of ± 1 over starburst-quench cycles, with bursty galaxies having higher than average SFR's $\sim 25\%$ of the time. On the other hand, more massive halos, with their deeper gravitational wells, are able to hold onto their gas reservoirs after a feedback event, so they instead undergo steady state star formation. The halo mass marking the transition between these two regimes depends on the assumed small-scale efficiency of star formation and the strength of feedback. Ref. [98] estimate the maximum halo mass that can host a starburst galaxy (SBG) to be $M_{\max}^{\text{SBG}} \sim 10^{10} - 10^{10.5} M_{\odot} h^{-1}$. Here, we would like to quantify (roughly) the maximum effect that we expect stochastic star formation to have on our results. We therefore adopt the high end of this range, $M_{\max}^{\text{SBG}} = 10^{11} M_{\odot} h^{-1}$.¹¹ Above $z = 11$ we have no halos this massive. In other words, with our assumed M_{\max}^{SBG} , all of our $z > 11$ sources are candidates for SBGs.

In our simplistic scheme, we begin with the UV-BRIGHT model described in §4 and the same halo mass-UV magnitude relation from the abundance matching procedure of the previous sections. At each snapshot of our hydrodynamics simulation (corresponding to $\Delta t \approx 10$ Myr), a random fraction, f_{SBG} , of all halos with masses $\leq M_{\max}^{\text{SBG}}$ are selected to be SBGs. We randomly swap the UV magnitude of each of these SBGs with a non-SBG that is $\Delta M_{UV} \sim 1$ brighter. This process is repeated at every hydrodynamical snapshot with a new random selection of SBGs and swappings. We note that the timescale of ~ 10 Myrs on which our SBGs flicker is consistent with the expected duration of starburst events in Ref. [98] and other works. Crucially, our approach preserves the *measured* UV luminosity function while implementing starburst events – albeit in a crude way. In what follows, we examine two stochastic star formation models. The first assumes $f_{\text{SBG}} = 25\%$, in line with Ref. [98], and is termed STOCHASTIC-SF: $f_{\text{SBG}} = 25\%$. The second takes a more extreme value of $f_{\text{SBG}} = 50\%$ and is labeled STOCHASTIC-SF: $f_{\text{SBG}} = 50\%$. We note $f_{\text{SBG}} = 50\%$ is the maximum value allowed in this approach for $z \gtrsim 11$. Because of our choice of M_{\max}^{SBG} , all galaxies in this epoch are SBG candidates, so $f_{\text{SBG}} > 50\%$ means there are more SBGs than non-SBG's, which would ruin our swapping scheme. Since the global ionizing emissivities of both STOCHASTIC-SF and UV-BRIGHT models are identical by construction, any differences in their pkSZ power owe solely to the changes in effective source clustering introduced by stochastic star formation, isolating exactly the effect we aim to test.

Figure 13 shows how stochastic star formation affects the pkSZ power spectra. In the left panel we compare D_{ℓ} in our STOCHASTIC-SF: $f_{\text{SBG}} = 25\%$ (dotted) and STOCHASTIC-SF: $f_{\text{SBG}} = 50\%$ models (dot-dashed) against the corresponding UV-BRIGHT models (dashed). For comparison, we also show a set of $\dot{n}_{\text{ion}} \propto L_{UV}$ models as the solid curves. Different colors denote different global reionization histories, as indicated in the legend. We can see the power spectra for each STOCHASTIC-SF: $f_{\text{SBG}} = 25\%$ model is only slightly flatter than the corresponding UV-BRIGHT model. In fact, around $\ell = 3,000$, these two sets of models are quite similar. This is emphasized in the right panel of Fig. 13, where we plot the normalized slope versus the amplitude of power at $\ell = 3,000$ (the same quantities plotted

¹¹For reference, in our abundance matching scheme from the previous sections, halos of this mass host galaxies with $M_{UV} \sim -20$ and -21.5 at $z = 6$ and 10 , respectively.

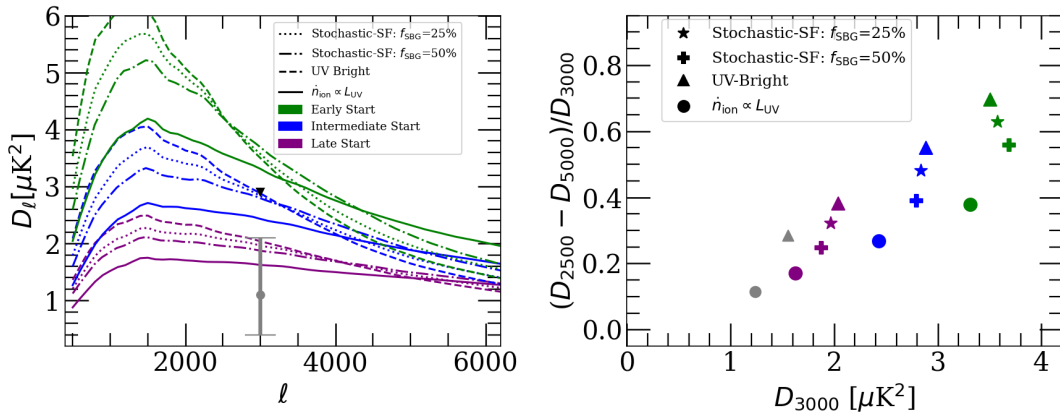


Figure 13. Testing the impact of stochastic star formation in $< 10^{11} M_\odot h^{-1}$ halos on the pkSZ power spectra. *Left:* D_ℓ for our STOCHASTIC-SF: $f_{\text{SBG}} = 25\%$ (dotted) and STOCHASTIC-SF: $f_{\text{SBG}} = 50\%$ models (dot-dashed) compared against UV-BRIGHT (dashed) and $\dot{n}_{\text{ion}} \propto L_{\text{UV}}$ (solid) source models for various reionization histories denoted by color. Both stochastic star formation models can be viewed as variations of the UV-BRIGHT model, but with stochasticity added using a prescription motivated by the semi-analytic model of Ref. [98] (see main text for details). *Right:* the normalized slope of the pkSZ power as a function of power amplitude at $\ell = 3,000$. The stars and crosses represent the STOCHASTIC-SF: $f_{\text{SBG}} = 25\%$ and STOCHASTIC-SF: $f_{\text{SBG}} = 50\%$ models respectively. The similarity between the STOCHASTIC-SF: $f_{\text{SBG}} = 25\%$ and UV-BRIGHT results suggest that stochasticity in a moderate fraction of galaxies likely has only a modest effect on the broad conclusions of the previous sections. However, the similarity between the STOCHASTIC-SF: $f_{\text{SBG}} = 50\%$ and $\dot{n}_{\text{ion}} \propto L_{\text{UV}}$ trend lines shows that a strong prevalence of stochastic star formation is partially degenerate with the effects of weaker source clustering.

in Fig. 11). Our STOCHASTIC-SF: $f_{\text{SBG}} = 25\%$ models (stars) have only \sim few % different D_{3000} , and $\sim 10-15\%$ lower values of $(D_{2500} - D_{5000})/D_{3000}$, compared to their corresponding UV-BRIGHT models (triangles). Overall, when implementing stochasticity into a moderate fraction of galaxies in the UV-BRIGHT models, we get results quite similar to the original UV-BRIGHT models. However, the D_ℓ slope continues to flatten as f_{SBG} increases. In fact, for histories with a LATE START or INTERMEDIATE START, the STOCHASTIC-SF: $f_{\text{SBG}} = 50\%$ models (pluses) have only slightly higher values of $(D_{2500} - D_{5000})/D_{3000}$ than the $\dot{n}_{\text{ion}} \propto L_{\text{UV}}$ models (circles), despite the latter allowing galaxies fainter than $M_{\text{UV}} = -18$ to contribute to reionization. This suggests an extreme prevalence of stochastic star formation can be partially degenerate with the inclusion of fainter galaxies in the effective clustering of ionizing sources and thus, the D_ℓ slope. A more complete exploration of this degeneracy between source modeling and stochasticity is left to future work.

The main takeaway from this test is that stochastic star formation among a moderate fraction of early galaxies probably has only a modest effect on the conclusions of the previous section. However, a very high stochastic fraction flattens the slope of D_ℓ significantly. Interpreting future measurements the pkSZ power spectrum slope may require modeling the effects of stochastic star formation.

5.3 Comparison to Previous Results

That the majority of D_{3000}^{pkSZ} is sourced at $x_{\text{HII}}^{\text{V}} \lesssim 40\%$ was also observed by Refs. [71, 83, 84]. Using a smaller set of RT simulations, Ref. [71] found that the fraction of power contributed at $x_{\text{HII}}^{\text{V}} \lesssim 40\%$ decreases if halos with masses $\sim 10^9 M_{\odot}$ drive reionization. However, they also found that this fraction remains above 50%, and does not decrease further, even when including contributions from atomic cooling halos down to masses of $10^8 M_{\odot}$. Ref. [83] found a similar result using the semi-numeric code 21CM-FAST. In that work, the exceptions were models in which the ionizing photon mean free path *in ionized gas* remains short enough to prevent the growth of ionized bubbles much larger than $\sim 10\text{Mpc}$ (i.e. until they merge with neighboring bubbles). In this scenario, smaller bubbles persist until much higher $x_{\text{HII}}^{\text{V}}$ and continue to contribute significantly to the pkSZ power at $\ell = 3000$ throughout reionization. Despite the differences in modeling between these works, they generally agree that in standard reionization scenarios driven by galaxies in atomic cooling halos, a majority of D_{3000}^{pkSZ} is sourced at $x_{\text{HII}}^{\text{V}} \lesssim 40\%$.

In contrast with our findings in §3.2.1, Ref. [71] found little change in D_{3000}^{pkSZ} with earlier starts to reionization. We argue that this discrepancy with our results is likely due to the relationship between their reionization histories and source models. For example, their “L2M1J1” model begins at $z \approx 25$ with the first $\approx 20\%$ of reionization driven by ionizing sources within minihalos down to masses $\sim 10^5 M_{\odot}$. As discussed in §4, less clustered sources generate fewer $\ell \sim 3000$ scale ionized bubbles at low- $x_{\text{HII}}^{\text{V}}$, reducing contributions to D_{3000}^{pkSZ} from those epochs. Indeed, the red curve in Figure 8 of Ref. [71] shows quite weak contributions to D_{3000}^{pkSZ} for this minihalo driven scenario all the way down to $z \sim 11$. At $z < 10$, when atomic cooling halos take over as the primary drivers of reionization, the higher $x_{\text{HII}}^{\text{V}}$ means their ionized regions grow larger than $\ell \sim 3000$ angular scales somewhat sooner than they otherwise would. This results in the model with minihalos having slightly lower D_{3000}^{pkSZ} contributions from $z \lesssim 10$, as seen in their Figure 8. It is possible that the slight loss of power from $z \lesssim 10$ offsets the mild early gains and makes D_{3000}^{pkSZ} effectively insensitive to the start of reionization. We emphasize this seems to be a result of the less clustered sources driving the earlier starts to reionization, not of minihalos in particular. Ref [71] sees similar behavior when comparing a scenario driven solely by high-mass atomic cooling halos ($\geq 2.2 \times 10^9 M_{\odot}$) against a model that includes sources within low-mass atomic cooling halos ($\geq 10^8 M_{\odot}$). This scenario serves as an important counterexample to our finding that D_{3000}^{pkSZ} is sensitive to the start of reionization.

Some recent analyses of the CMB temperature and lensing data within the ΛCDM model find a preference for a larger CMB optical depth of $\tau_{\text{es}} \sim 0.09$ when the Baryon Acoustic Oscillation data from DESI [105] is included [106, 107]¹². However, using a suite of semi-numeric simulations with the end of reionization set to be consistent with Ly α forest constraints, Ref. [17] pointed out such high τ_{es} is in $\gtrsim 2\sigma$ tension with the low value of D_{3000}^{pkSZ} measured by SPT. We emphasize that this tension only occurs because of the strict constraints on the end of reionization from the Ly α forest. The scenario described in the previous paragraph – where reionization begins early, driven by weakly clustered sources – could plausibly satisfy all three constraints. The early start to reionization yields a high τ_{es} , and it is possible that the rarity of $\ell \sim 3000$ scale ionized regions generated by the minihalo sources keeps D_{3000}^{pkSZ} low, even when reionization ends around $z \sim 5.5$ (as required by the Ly α

¹²Such analyses do not include the low- ℓ EE polarization data from *Planck*, which is the primary observational evidence for $\tau_{\text{es}} \sim 0.06$

forest). This discussion further underscores the need to clarify the role of weakly clustered sources at the beginning of reionization to properly interpret D_{3000}^{pkSZ} (see Ref. [71]). As discussed in §4.2.2, a signature of weak source clustering is more pkSZ power at larger ℓ , so measurements from future small scale CMB experiments are a promising way to gain insights into the earliest sources of reionization.

6 Conclusion

Over the past decade, advances in Ly α forest observations at $z > 5$ have brought reionization’s last phases into focus. Indeed, forest measurements now provide more than a simple lower limit on the end of reionization; they place stringent constraints on its timing (see e.g. the discussion in [17]). These constraints will continue to improve as more high- z quasars are discovered in wide-field cosmological surveys and followed up to obtain high signal-to-noise spectra. On the other hand, future CMB experiments have the potential to provide robust constraints on the highly uncertain earlier phases of reionization. Better constraining the start of reionization would, in turn, provide valuable insights into the nature and ionizing properties of JWST sources detected at these epochs. We have used a suite of radiative transfer simulations to explore how the pkSZ power spectrum could be used as such a window when combined with Ly α forest constraints on reionization’s end. Our main results are summarized as follows:

- For the galaxy-sourced models considered in this paper (with $M_{\text{min}} \geq 10^9 h^{-1} M_{\odot}$), The pkSZ power at $\ell \sim 3,000$ receives most of its contribution from the first 40% of reionization.
- For a fixed model of the ionizing source clustering, when the timing of reionization’s end is constrained by measurements of the Ly α forest mean transmission at $z = 5 - 6$, the amplitude of the pkSZ power spectra, D_{3000}^{pkSZ} , strongly correlates with the beginning epoch of reionization (defined here to be the redshift at which $x_{\text{HII}} = 5\%$, z_{05}). Imposing physically motivated limits on how quickly the global ionizing emissivity can grow, existing and future pkSZ measurements can be translated to model-dependent upper limits on the cumulative number of ionizing photons emitted per hydrogen atom by the high- z source population, $N_{\gamma/H}(z \gtrsim 8)$.
- Varying the assumed relationship between dark matter halos and the ionizing outputs of their host galaxies (i.e. varying the assumed source clustering) introduces a significant amount of scatter into the correlations between D_{3000}^{pkSZ} and both z_{05} and $N_{\gamma/H}$. This owes to a degeneracy in D_{3000}^{pkSZ} between the morphology of reionization (set by the clustering of ionizing sources) and the early reionization history. Much like variations in the reionization history, various source clustering models imprint differences in the pkSZ power within the first 30% of reionization.
- We demonstrated that the aforementioned degeneracy can be partly broken in at least two ways: (1) by incorporating additional constraints in the form of the observed spatial fluctuations in the Ly α forest opacity at $5 \lesssim z \lesssim 6$; (2) by incorporating information about the shape of the pkSZ power spectrum around $\ell = 3,000$. The shape of the power spectrum is sensitive to the clustering of the ionizing sources, with less clustered sources yielding flatter power spectra. This latter method is most useful in scenarios with larger amplitudes of $D_{3,000}^{\text{pkSZ}}$.

- We performed tests to explore how sensitive these conclusions are to possible time-evolution in the emissivity-halo connection, as well as highly stochastic ionizing emissions at high redshift. These tests suggest that such effects are unlikely to change our broad conclusions. However, stochastic star formation among high fraction ($> 50\%$) of galaxies can flatten the pkSZ power spectrum, complicating its interpretation.

Future CMB experiments such as Simons Observatory and CMB-S4, in combination with ever-improving constraints from the Ly α forest, have the potential to constrain the ionization state of the early IGM. Our results suggest that a synthesis of CMB, Ly α forest, and JWST observations can yield deeper insights into the ionizing sources near cosmic dawn.

Acknowledgments

The authors thank Hy Trac for generously providing access to his cosmological hydrodynamics code. The authors also thank Paul Shapiro and Matt McQuinn for helpful discussions. A.D. acknowledges support from grants NASA 19-ATP19-0191 and NSF AST-2045600. All computations were made possible by NSF ACCESS allocations TG-PHY210041 and TG-PHY230063.

A Comparing pkSZ for Full and Reduced Speed of Light Runs

To confirm the robustness of our method of remapping the emissivities from simulations employing the reduced speed of light approximation, we compare to results from simulations that use the full speed of light. Specifically, we take two reionization histories from Ref [37], one with a late start and a second with an early start ($z_{05} \sim 9.3$ and ~ 12.5 respectively). Both use the same $\dot{n}_{\text{ion}} \propto L_{\text{UV}}$ source model used in this work and were calibrated in full speed of light simulations to agree with the measurements of the Ly α forest mean flux from Ref. [15]. We find the equivalent emissivities using the inversions of Eqs. 2.1 and 2.2 to use in $\tilde{c}/c=0.2$ simulations. In Fig. 14 we compare the pkSZ power spectra calculated from the original full speed of light simulations against those from new $\tilde{c}/c = 0.2$ simulations with remapped emissivities. In both the early and late starting cases the $\tilde{c}/c = 0.2$ runs gained $\sim 0.026 \mu\text{K}^2$ in D_{3000}^{pkSZ} which corresponds to a difference of $\lesssim 1.5\%$. As such, we expect our results to be near identical had we used full speed of light simulations.

References

- [1] G. Kulkarni, L.C. Keating, M.G. Haehnelt, S.E.I. Bosman, E. Puchwein, J. Chardin et al., *Large Ly α opacity fluctuations and low CMB τ in models of late reionization with large islands of neutral hydrogen extending to $z < 5.5$* , *Monthly Notices of the Royal Astronomical Society* **485** (2019) L24 [[1809.06374](#)].
- [2] L.C. Keating, L.H. Weinberger, G. Kulkarni, M.G. Haehnelt, J. Chardin and D. Aubert, *Long troughs in the Lyman- α forest below redshift 6 due to islands of neutral hydrogen*, *Monthly Notices of the Royal Astronomical Society* **491** (2020) 1736 [[1905.12640](#)].
- [3] F. Nasir and A. D’Aloisio, *Observing the tail of reionization: neutral islands in the $z = 5.5$ Lyman- α forest*, *Monthly Notices of the Royal Astronomical Society* **494** (2020) 3080 [[1910.03570](#)].

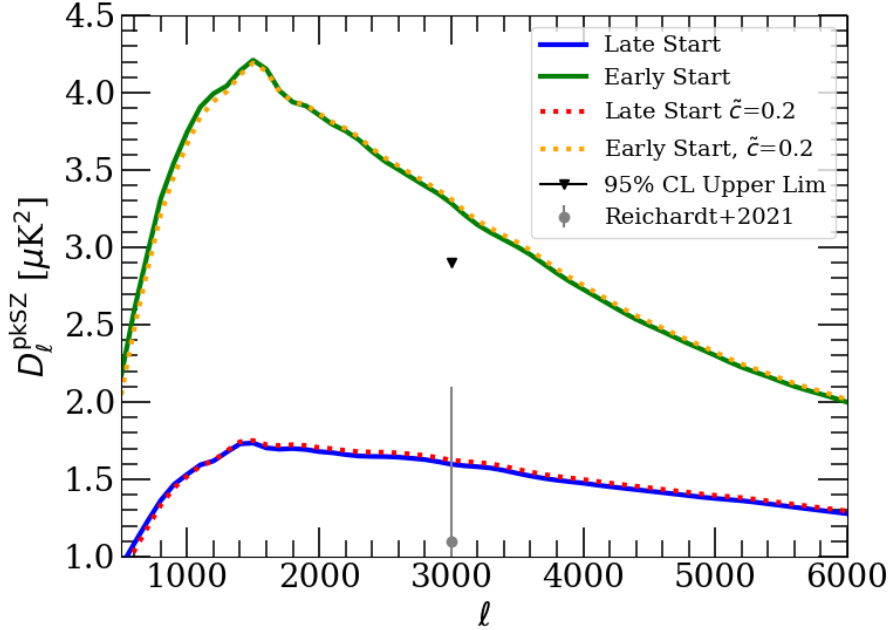


Figure 14. Comparing the pkSZ power spectrum from full speed of light ($\tilde{c}/c = 1$) simulations against $\tilde{c}/c = 0.2$ reduced speed of light simulations with remapped emissivities given by inversions of Eq. 2.1 and Eq. 2.2. The pkSZ power spectra for $\tilde{c}/c = 1$ ($\tilde{c}/c = 0.2$) simulations of the early starting reionization history is given by the solid-green (orange-dotted) curve, and D_{ℓ}^{pkSZ} for the late starting history is given by the solid-blue (red-dotted) curve. For both histories we find $\lesssim 1.5\%$ difference in D_{3000}^{pkSZ} due to our use of reduced speed of light simulations.

- [4] Y. Zhu, G.D. Becker, S.E.I. Bosman, L.C. Keating, H.M. Christenson, E. Bañados et al., *Chasing the Tail of Cosmic Reionization with Dark Gap Statistics in the Ly α Forest over $5 < z < 6$* , *The Astrophysical Journal* **923** (2021) 223 [2109.06295].
- [5] Y. Zhu, G.D. Becker, S.E.I. Bosman, L.C. Keating, V. D’Odorico, R.L. Davies et al., *Long Dark Gaps in the Ly β Forest at $z < 6$: Evidence of Ultra-late Reionization from XQR-30 Spectra*, *The Astrophysical Journal* **932** (2022) 76 [2205.04569].
- [6] G.D. Becker, A. D’Aloisio, H.M. Christenson, Y. Zhu, G. Worseck and J.S. Bolton, *The mean free path of ionizing photons at $5 < z < 6$: evidence for rapid evolution near reionization*, *Monthly Notices of the Royal Astronomical Society* **508** (2021) 1853 [2103.16610].
- [7] Y. Zhu, G.D. Becker, H.M. Christenson, A. D’Aloisio, S.E.I. Bosman, T. Bakx et al., *Probing Ultralate Reionization: Direct Measurements of the Mean Free Path over $5 < z < 6$* , *The Astrophysical Journal* **955** (2023) 115 [2308.04614].
- [8] P. Gaikwad, M.G. Haehnelt, F.B. Davies, S.E.I. Bosman, M. Molaro, G. Kulkarni et al., *Measuring the photoionization rate, neutral fraction, and mean free path of H I ionizing photons at $4.9 \leq z \leq 6.0$ from a large sample of XShooter and ESI spectra*, *Monthly Notices of the Royal Astronomical Society* **525** (2023) 4093 [2304.02038].
- [9] F.B. Davies, S.E.I. Bosman, P. Gaikwad, F. Nasir, J.F. Hennawi, G.D. Becker et al., *Constraints on the Evolution of the Ionizing Background and Ionizing Photon Mean Free Path at the End of Reionization*, *The Astrophysical Journal* **965** (2024) 134 [2312.08464].
- [10] J.T. Roth, A. D’Aloisio, C. Cain, B. Wilson, Y. Zhu and G.D. Becker, *The effect of*

reionization on direct measurements of the mean free path, *Monthly Notices of the Royal Astronomical Society* **530** (2024) 5209 [2311.06348].

- [11] S. Satyavolu, G. Kulkarni, L.C. Keating and M.G. Haehnelt, *Robustness of direct measurements of the mean free path of ionizing photons in the epoch of reionization*, *Monthly Notices of the Royal Astronomical Society* **533** (2024) 676 [2311.06344].
- [12] G.D. Becker, J.S. Bolton, Y. Zhu and S. Hashemi, *Damping wing absorption associated with a giant Ly α trough at $z < 6$: direct evidence for late-ending reionization*, *arXiv e-prints* (2024) arXiv:2405.08885 [2405.08885].
- [13] Y. Zhu, G.D. Becker, S.E.I. Bosman, C. Cain, L.C. Keating, F. Nasir et al., *Damping Wing-Like Features in the Stacked Ly α Forest: Potential Neutral Hydrogen Islands at $z < 6$* , *arXiv e-prints* (2024) arXiv:2405.12275 [2405.12275].
- [14] B. Spina, S.E.I. Bosman, F.B. Davies, P. Gaikwad and Y. Zhu, *Damping wings in the Lyman- α forest: a model-independent measurement of the neutral fraction at $5.4 < z < 6.1$* , *arXiv e-prints* (2024) arXiv:2405.12273 [2405.12273].
- [15] S.E.I. Bosman, F.B. Davies, G.D. Becker, L.C. Keating, R.L. Davies, Y. Zhu et al., *Hydrogen reionization ends by $z = 5.3$: Lyman- α optical depth measured by the XQR-30 sample*, *Monthly Notices of the Royal Astronomical Society* **514** (2022) 55 [2108.03699].
- [16] Y. Qin, A. Mesinger, D. Prelogović, G. Becker, M. Bischetti, S. Bosman et al., *Percent-level timing of reionisation: Self-consistent, implicit-likelihood inference from XQR-30+ Ly α forest data*, *Publ. Astron. Soc. As* **42** (2025) e049 [2412.00799].
- [17] C. Cain, A. Van Engelen, K.S. Croker, D. Kramer, A. D'Aloisio and G. Lopez, *The CMB optical depth constrains the duration of reionization*, *arXiv e-prints* (2025) arXiv:2505.15899 [2505.15899].
- [18] C.T. Donnan, D.J. McLeod, J.S. Dunlop, R.J. McLure, A.C. Carnall, R. Begley et al., *The evolution of the galaxy UV luminosity function at redshifts $z = 8 - 15$ from deep JWST and ground-based near-infrared imaging*, *Monthly Notices of the Royal Astronomical Society* **518** (2023) 6011 [2207.12356].
- [19] R. Bouwens, G. Illingworth, P. Oesch, M. Stefanon, R. Naidu, I. van Leeuwen et al., *UV luminosity density results at $z > 8$ from the first JWST/NIRCam fields: limitations of early data sets and the need for spectroscopy*, *Monthly Notices of the Royal Astronomical Society* **523** (2023) 1009 [2212.06683].
- [20] M. Castellano, A. Fontana, T. Treu, E. Merlin, P. Santini, P. Bergamini et al., *Early Results from GLASS-JWST. XIX. A High Density of Bright Galaxies at $z \approx 10$ in the A2744 Region*, *The Astrophysical Journal Letters* **948** (2023) L14 [2212.06666].
- [21] P.G. Pérez-González, L. Costantin, D. Langeroodi, P. Rinaldi, M. Annunziatella, O. Ilbert et al., *Life beyond 30: Probing the $-20 < M_{UV} < -17$ Luminosity Function at $8 < z < 13$ with the NIRCam Parallel Field of the MIRI Deep Survey*, *The Astrophysical Journal Letters* **951** (2023) L1 [2302.02429].
- [22] G.C.K. Leung, M.B. Bagley, S.L. Finkelstein, H.C. Ferguson, A.M. Koekemoer, P.G. Pérez-González et al., *NGDEEP Epoch 1: The Faint End of the Luminosity Function at $z 9-12$ from Ultradeep JWST Imaging*, *The Astrophysical Journal Letters* **954** (2023) L46 [2306.06244].
- [23] D.J. McLeod and Donnan, C. T. and McLure, R. J. and Dunlop, J. S. and Magee, D. and Begley, R. and Carnall, A. C. and Cullen, F. and Ellis, R. S. and Hamadouche, M. L. and Stanton, T. M., *The galaxy UV luminosity function at $z = 11$ from a suite of public JWST ERS, ERO, and Cycle-1 programs*, *Monthly Notices of the Royal Astronomical Society* **527** (2024) 5004 [2304.14469].

- [24] S.L. Finkelstein, G.C.K. Leung, M.B. Bagley, M. Dickinson, H.C. Ferguson, C. Papovich et al., *The Complete CEERS Early Universe Galaxy Sample: A Surprisingly Slow Evolution of the Space Density of Bright Galaxies at $z \sim 8.5\text{--}14.5$* , *The Astrophysical Journal Letters* **969** (2024) L2 [2311.04279].
- [25] N.J. Adams, C.J. Conselice, D. Austin, T. Harvey, L. Ferreira, J. Trussler et al., *EPOCHS. II. The Ultraviolet Luminosity Function from $7.5 < z < 13.5$ Using 180 arcmin^2 of Deep, Blank Fields from the PEARLS Survey and Public JWST Data*, *The Astrophysical Journal* **965** (2024) 169 [2304.13721].
- [26] L. Whitler, D.P. Stark, M.W. Topping, B. Robertson, M. Rieke, K.N. Hainline et al., *The *z*rsim9 galaxy UV luminosity function from the JWST Advanced Deep Extragalactic Survey: insights into early galaxy evolution and reionization*, *arXiv e-prints* (2025) arXiv:2501.00984 [2501.00984].
- [27] P. Arrabal Haro, M. Dickinson, S.L. Finkelstein, J.S. Kartaltepe, C.T. Donnan, D. Burgarella et al., *Confirmation and refutation of very luminous galaxies in the early Universe*, *Nature* **622** (2023) 707 [2303.15431].
- [28] R. Endsley, D.P. Stark, L. Whitler, M.W. Topping, B.D. Johnson, B. Robertson et al., *The star-forming and ionizing properties of dwarf z 6–9 galaxies in JADES: insights on bursty star formation and ionized bubble growth*, *Monthly Notices of the Royal Astronomical Society* **533** (2024) 1111 [2306.05295].
- [29] A.J. Pahl, M.W. Topping, A. Shapley, R. Sanders, N.A. Reddy, L. Clarke et al., *A spectroscopic analysis of the ionizing photon production efficiency in JADES and CEERS: implications for the ionizing photon budget*, *arXiv e-prints* (2024) arXiv:2407.03399 [2407.03399].
- [30] C. Simmonds, S. Tacchella, K. Hainline, B.D. Johnson, W. McClymont, B. Robertson et al., *Low-mass bursty galaxies in JADES efficiently produce ionizing photons and could represent the main drivers of reionization*, *Monthly Notices of the Royal Astronomical Society* **527** (2024) 6139 [2310.01112].
- [31] B.E. Robertson, R.S. Ellis, S.R. Furlanetto and J.S. Dunlop, *Cosmic Reionization and Early Star-forming Galaxies: A Joint Analysis of New Constraints from Planck and the Hubble Space Telescope*, *The Astrophysical Journal Letters* **802** (2015) L19 [1502.02024].
- [32] S.L. Finkelstein, A. D’Aloisio, J.-P. Paardekooper, J. Ryan, Russell, P. Behroozi, K. Finlator et al., *Conditions for Reionizing the Universe with a Low Galaxy Ionizing Photon Escape Fraction*, *The Astrophysical Journal* **879** (2019) 36 [1902.02792].
- [33] H. Atek, I. Labbé, L.J. Furtak, I. Chemerynska, S. Fujimoto, D.J. Setton et al., *Most of the photons that reionized the Universe came from dwarf galaxies*, *Nature* **626** (2024) 975 [2308.08540].
- [34] J.B. Muñoz, J. Mirocha, J. Chisholm, S.R. Furlanetto and C. Mason, *Reionization after JWST: a photon budget crisis?*, *Monthly Notices of the Royal Astronomical Society* **535** (2024) L37 [2404.07250].
- [35] J. Chisholm, A. Saldana-Lopez, S. Flury, D. Schaerer, A. Jaskot, R. Amorín et al., *The far-ultraviolet continuum slope as a Lyman Continuum escape estimator at high redshift*, *Monthly Notices of the Royal Astronomical Society* **517** (2022) 5104 [2207.05771].
- [36] C. Simmonds, S. Tacchella, K. Hainline, B.D. Johnson, D. Puskás, B. Robertson et al., *Ionizing properties of galaxies in JADES for a stellar mass complete sample: resolving the cosmic ionizing photon budget crisis at the Epoch of Reionization*, *Monthly Notices of the Royal Astronomical Society* **535** (2024) 2998 [2409.01286].
- [37] C. Cain, G. Lopez, A. D’Aloisio, J.B. Munoz, R.A. Jansen, R.A. Windhorst et al., *Chasing*

the beginning of reionization in the JWST era, *arXiv e-prints* (2024) arXiv:2409.02989 [2409.02989].

- [38] HERA Collaboration, Z. Abdurashidova, T. Adams, J.E. Aguirre, P. Alexander, Z.S. Ali et al., *Improved Constraints on the 21 cm EoR Power Spectrum and the X-Ray Heating of the IGM with HERA Phase I Observations*, *The Astrophysical Journal* **945** (2023) 124 [2210.04912].
- [39] C.D. Nunhokee, D. Null, C.M. Trott, N. Barry, Y. Qin, R.B. Wayth et al., *Limits on the 21 cm power spectrum at $z=6.5-7.0$ from MWA observations*, *arXiv e-prints* (2025) arXiv:2505.09097 [2505.09097].
- [40] H. Umeda, M. Ouchi, K. Nakajima, Y. Harikane, Y. Ono, Y. Xu et al., *JWST Measurements of Neutral Hydrogen Fractions and Ionized Bubble Sizes at $z = 7 - 12$ Obtained with Ly α Damping Wing Absorptions in 26 Bright Continuum Galaxies*, *arXiv e-prints* (2023) arXiv:2306.00487 [2306.00487].
- [41] J. Witstok, P. Jakobsen, R. Maiolino, J.M. Helton, B.D. Johnson, B.E. Robertson et al., *Witnessing the onset of reionization through Lyman-alpha emission at redshift 13*, *Nature* **639** (2025) 897.
- [42] C.A. Mason, Z. Chen, D.P. Stark, T.-Y. Lu, M. Topping and M. Tang, *Constraints on the $z \sim 6 - 13$ intergalactic medium from JWST spectroscopy of Lyman-alpha damping wings in galaxies*, *arXiv e-prints* (2025) arXiv:2501.11702 [2501.11702].
- [43] S. Hassan and M. Gronke, *Can Galaxy Evolution Mimic Cosmic Reionization?*, *The Astrophysical Journal* **908** (2021) 219 [2010.00023].
- [44] Planck Collaboration, N. Aghanim, Y. Akrami, M. Ashdown, J. Aumont, C. Baccigalupi et al., *Planck 2018 results. VI. Cosmological parameters*, *Astronomy and Astrophysics* **641** (2020) A6 [1807.06209].
- [45] M. Tristram, A.J. Banday, M. Douspis, X. Garrido, K.M. Górski, S. Henrot-Versillé et al., *Cosmological parameters derived from the final Planck data release (PR4)*, *Astronomy and Astrophysics* **682** (2024) A37 [2309.10034].
- [46] X. Wu, M. McQuinn, D. Eisenstein and V. Iršič, *The high-redshift tail of stellar reionization in Λ CDM is beyond the reach of the low- l CMB*, *Monthly Notices of the Royal Astronomical Society* **508** (2021) 2784 [2105.08737].
- [47] C.L. Reichardt, S. Patil, P.A.R. Ade, A.J. Anderson, J.E. Austermann, J.S. Avva et al., *An improved measurement of the secondary cosmic microwave background anisotropies from the SPT-SZ + SPTpol surveys*, 2002.06197.
- [48] E. Calabrese, R. Hložek, N. Battaglia, J.R. Bond, F. de Bernardis, M.J. Devlin et al., *Precision epoch of reionization studies with next-generation CMB experiments*, *J. Cosmol. Astropart. Phys.* **2014** (2014) 010.
- [49] L.D. Shaw, D.H. Rudd and D. Nagai, *Deconstructing the kinetic SZ power spectrum*, *Astrophys. J.* **756** (2012) 15.
- [50] B. Beringue, K.M. Surrao, J.C. Hill, Z. Atkins, N. Battaglia, B. Bolliet et al., *The atacama cosmology telescope: DR6 power spectrum foreground model and validation*, *arXiv [astro-ph.CO]* (2025) .
- [51] D. Jain, T.R. Choudhury, S. Raghunathan and S. Mukherjee, *Probing the physics of reionization using k SZ power spectrum from current and upcoming CMB surveys*, 2311.00315.
- [52] C. Cain and A. D’Aloisio, *FlexRT – a fast and flexible cosmological radiative transfer code for reionization studies I: Code validation*, *arXiv [astro-ph.CO]* (2024) .
- [53] T. Abel and B.D. Wandelt, *Adaptive ray tracing for radiative transfer around point sources*, *Monthly Notices of the Royal Astronomical Society* **330** (2002) L53 [astro-ph/0111033].

- [54] H. Trac and R. Cen, *Radiative transfer simulations of cosmic reionization. i. methodology and initial results*, *Astrophys. J.* **671** (2007) 1.
- [55] C. Cain, A. D’Aloisio, N. Gangolli and G.D. Becker, *A short mean free path at $z = 6$ favors late and rapid reionization by faint galaxies*, *ApJL* **917** (2021) L37.
- [56] C. Cain, A. D’Aloisio, N. Gangolli and M. McQuinn, *The morphology of reionization in a dynamically clumpy universe*, *Mon. Not. R. Astron. Soc.* **522** (2023) 2047.
- [57] A. D’Aloisio, M. McQuinn, O. Maupin, F.B. Davies, H. Trac, S. Fuller et al., *Heating of the Intergalactic Medium by Hydrogen Reionization*, *The Astrophysical Journal* **874** (2019) 154 [1807.09282].
- [58] A. D’Aloisio, M. McQuinn, F.B. Davies and S.R. Furlanetto, *Large fluctuations in the high-redshift metagalactic ionizing background*, *Monthly Notices of the Royal Astronomical Society* **473** (2018) 560 [1611.02711].
- [59] H. Trac and U.-L. Pen, *A moving frame algorithm for high mach number hydrodynamics*, *New Astron.* **9** (2004) 443.
- [60] C. Cain, A. D’Aloisio, G. Lopez, N. Gangolli and J.T. Roth, *On the rise and fall of galactic ionizing output at the end of reionization*, *Monthly Notices of the Royal Astronomical Society* **531** (2024) 1951 [2311.13638].
- [61] H. Trac, R. Cen and P. Mansfield, *SCORCH I: The Galaxy-Halo Connection in the First Billion Years*, *The Astrophysical Journal* **813** (2015) 54 [1507.02685].
- [62] N. Gangolli, A. D’Aloisio, C. Cain, G.D. Becker and H. Christenson, *On the correlation between Ly α forest opacity and galaxy density in late reionization models*, *arXiv [astro-ph.CO]* (2024) arXiv:2408.08358.
- [63] R.J. Bouwens, P.A. Oesch, M. Stefanon, G. Illingworth, I. Labbé, N. Reddy et al., *New Determinations of the UV Luminosity Functions from $z = 9$ to $z = 2$ Show a Remarkable Consistency with Halo Growth and a Constant Star Formation Efficiency*, *The Astronomical Journal* **162** (2021) 47 [2102.07775].
- [64] N.J. Adams, C.J. Conselice, D. Austin, T. Harvey, L. Ferreira, J. Trussler et al., *EPOCHS. II. the ultraviolet luminosity function from $7.5 < z < 13.5$ using 180 arcmin² of deep, blank fields from the PEARLS survey and public JWST data*, *Astrophys. J.* **965** (2024) 169.
- [65] C.T. Donnan, R.J. McLure, J.S. Dunlop, D.J. McLeod, D. Magee, K.Z. Arellano-Córdova et al., *JWST PRIMER: A new multi-field determination of the evolving galaxy UV luminosity function at redshifts $z \simeq 9 - 15$* , *arXiv [astro-ph.GA]* (2024) 3222.
- [66] T. Tepper-García, *Voigt profile fitting to quasar absorption lines: an analytic approximation to the Voigt-Hjerting function*, *Monthly Notices of the Royal Astronomical Society* **369** (2006) 2025 [astro-ph/0602124].
- [67] N.Y. Gnedin, *On the Proper Use of the Reduced Speed of Light Approximation*, *The Astrophysical Journal* **833** (2016) 66 [1607.07869].
- [68] N. Deparis, D. Aubert, P. Ocvirk, J. Chardin and J. Lewis, *Impact of the reduced speed of light approximation on ionization front velocities in cosmological simulations of the epoch of reionization*, *Astronomy and Astrophysics* **622** (2019) A142 [1803.01634].
- [69] C. Cain, *Accurate simulations of reionization using the reduced speed of light approximation*, *arXiv [astro-ph.CO]* (2024) .
- [70] R.A. Sunyaev and Y.B. Zeldovich, *The velocity of clusters of galaxies relative to the microwave background. the possibility of its measurement*, *Mon. Not. R. Astron. Soc.* **190** (1980) 413.
- [71] H. Park, P.R. Shapiro, E. Komatsu, I.T. Iliev, K. Ahn and G. Mellema, *The kinetic*

sunyaev-zel'dovich effect as a probe of the physics of cosmic reionization: the effect of self-regulated reionization, arXiv [astro-ph.CO] (2013) .

- [72] C.-P. Ma and J.N. Fry, *Nonlinear kinetic Sunyaev-Zeldovich effect*, *Phys. Rev. Lett.* **88** (2002) 211301.
- [73] A. Lewis, A. Challinor and A. Lasenby, *Efficient computation of cosmic microwave background anisotropies in closed Friedmann-Robertson-Walker models*, *Astrophys. J.* **538** (2000) 473.
- [74] M.A. Alvarez, *The kinetic Sunyaev-Zel'dovich effect from reionization: Simulated full-sky maps at arcminute resolution*, *Astrophys. J.* **824** (2016) 118.
- [75] C.L. Reichardt, S. Patil, P.A.R. Ade, A.J. Anderson, J.E. Austermann, J.S. Avva et al., *An improved measurement of the secondary cosmic microwave background anisotropies from the SPT-SZ + SPTpol surveys, arXiv [astro-ph.CO] (2020) .*
- [76] L.D. Shaw, D.H. Rudd and D. Nagai, *Deconstructing the kinetic SZ power spectrum*, *Astrophys. J.* **756** (2012) 15.
- [77] G.D. Becker and J.S. Bolton, *New measurements of the ionizing ultraviolet background over $2 < z < 5$ and implications for hydrogen reionization*, *Monthly Notices of the Royal Astronomical Society* **436** (2013) 1023 [[1307.2259](#)].
- [78] M. Tristram, A.J. Banday, M. Douspis, X. Garrido, K.M. Górski, S. Henrot-Versillé et al., *Cosmological parameters derived from the final Planck data release (PR4)*, *Astronomy and Astrophysics* **682** (2024) A37 [[2309.10034](#)].
- [79] N. Battaglia, A. Natarajan, H. Trac, R. Cen and A. Loeb, *Reionization on large scales III: Predictions for low- ℓ cosmic microwave background polarization and high- ℓ kinetic Sunyaev-Zel'dovich observables*, [1211.2832](#).
- [80] N. Chen, H. Trac, S. Mukherjee and R. Cen, *Patchy kinetic Sunyaev-Zel'dovich effect with controlled reionization history and morphology*, [2203.04337](#).
- [81] I. Nikolić, A. Mesinger, Y. Qin and A. Gorce, *Inferring reionization and galaxy properties from the patchy kinetic Sunyaev-Zel'dovich signal*, *arXiv e-prints* (2023) arXiv:2307.01265.
- [82] M. McQuinn, S.R. Furlanetto, L. Hernquist, O. Zahn and M. Zaldarriaga, *The kinetic Sunyaev-Zel'dovich effect from reionization*, [astro-ph/0504189](#).
- [83] A. Mesinger, M. McQuinn and D.N. Spergel, *The kinetic Sunyaev-Zel'dovich signal from inhomogeneous reionization: a parameter space study*, *Mon. Not. R. Astron. Soc.* **422** (2012) 1403.
- [84] A. Gorce, S. Ilić, M. Douspis, D. Aubert and M. Langer, *Improved constraints on reionisation from CMB observations: A parameterisation of the kSZ effect*, *arXiv [astro-ph.CO] (2020) .*
- [85] T.R. Choudhury, S. Mukherjee and S. Paul, *Cosmic microwave background constraints on a physical model of reionization*, *Mon. Not. R. Astron. Soc. Lett.* **501** (2020) L7.
- [86] R.P. Naidu, S. Tacchella, C.A. Mason, S. Bose, P.A. Oesch and C. Conroy, *Rapid reionization by the oligarchs: The case for massive, UV-bright, star-forming galaxies with high escape fractions*, *Astrophys. J.* **892** (2020) 109.
- [87] J. Matthee, D. Sobral, M. Hayes, G. Pezzulli, M. Gronke, D. Schaerer et al., *The X-SHOOTER lyman α survey at $z = 2$ (XLS-z2) i: what makes a galaxy a lyman α emitter?*, *Mon. Not. R. Astron. Soc.* **505** (2021) 1382.
- [88] S. Paul, S. Mukherjee and T.R. Choudhury, *Inevitable imprints of patchy reionization on the cosmic microwave background anisotropy*, [2005.05327](#).
- [89] I.T. Iliev, G. Mellema, P.R. Shapiro and U.-L. Pen, *Self-regulated reionization*, *Monthly Notices of the Royal Astronomical Society* **376** (2007) 534 [[astro-ph/0607517](#)].

- [90] P. Ocvirk, J.S.W. Lewis, N. Gillet, J. Chardin, D. Aubert, N. Deparis et al., *Lyman-alpha opacities at $z = 4-6$ require low mass, radiatively-suppressed galaxies to drive cosmic reionization*, *Monthly Notices of the Royal Astronomical Society* **507** (2021) 6108 [2105.01663].
- [91] A. Kravtsov and V. Belokurov, *Stochastic star formation and the abundance of $z > 10$ UV-bright galaxies*, *arXiv [astro-ph.GA]* (2024) .
- [92] T.J. Looser, F. D'Eugenio, R. Maiolino, S. Tacchella, M. Curti, S. Arribas et al., *JADES: Differing assembly histories of galaxies – observational evidence for bursty SFHs and (mini-)quenching in the first billion years of the universe*, *arXiv [astro-ph.GA]* (2023) A88.
- [93] V. Kokorev, O.A.C. Ortiz, A.J. Taylor, S.L. Finkelstein, P.A. Haro, M. Dickinson et al., *Capser observations of two uv-bright galaxies at $z > 10$. more evidence for bursting star formation in the early universe*, *arXiv [astro-ph.GA]* (2025) arXiv:2504.12504.
- [94] D.P. Stark, M.W. Topping, R. Endsley and M. Tang, *Observations of the first galaxies in the era of JWST*, *arXiv [astro-ph.GA]* (2025) .
- [95] J.W. Cole, C. Papovich, S.L. Finkelstein, M.B. Bagley, M. Dickinson, K.G. Iyer et al., *CEERS: Increasing scatter along the star-forming main sequence indicates early galaxies form in bursts*, *arXiv [astro-ph.GA]* (2023) .
- [96] M.W. Topping, D.P. Stark, P. Senchyna, Z. Chen, A. Zitrin, R. Endsley et al., *Deep rest-UV JWST/NIRSpec spectroscopy of early galaxies: the demographics of CIV and N-emitters in the reionization era*, *arXiv [astro-ph.GA]* (2024) .
- [97] L. Ciesla, D. Elbaz, O. Ilbert, V. Buat, B. Magnelli, D. Narayanan et al., *Identification of a transition from stochastic to secular star formation around $z = 9$ with JWST*, *arXiv [astro-ph.GA]* (2023) A128.
- [98] S.R. Furlanetto and J. Mirocha, *Bursty star formation during the cosmic dawn driven by delayed stellar feedback*, *arXiv [astro-ph.GA]* (2021) .
- [99] J. Mirocha and S.R. Furlanetto, *Balancing the efficiency and stochasticity of star formation with dust extinction in $z > 10$ galaxies observed by JWST*, *arXiv [astro-ph.GA]* (2022) .
- [100] G. Sun, C.-A. Faucher-Giguère, C.C. Hayward, X. Shen, A. Wetzel and R.K. Cochrane, *Bursty star formation naturally explains the abundance of bright galaxies at cosmic dawn*, *arXiv [astro-ph.GA]* (2023) .
- [101] G. Sun, C.-A. Faucher-Giguère, C.C. Hayward and X. Shen, *Seen and unseen: bursty star formation and its implications for observations of high-redshift galaxies with JWST*, *arXiv [astro-ph.GA]* (2023) .
- [102] G. Sun, J.B. Muñoz, J. Mirocha and C.-A. Faucher-Giguère, *Constraining bursty star formation histories with galaxy UV and H α luminosity functions and clustering*, *arXiv [astro-ph.GA]* (2024) .
- [103] Z.L. Andelman, R. Teyssier and A. Dekel, *On the origin of the high star-formation efficiency in massive galaxies at cosmic dawn*, *arXiv [astro-ph.GA]* (2024) .
- [104] V. Gelli, C. Mason and C.C. Hayward, *The impact of mass-dependent stochasticity at cosmic dawn*, *arXiv [astro-ph.GA]* (2024) .
- [105] DESI Collaboration, M. Abdul-Karim, J. Aguilar, S. Ahlen, S. Alam, L. Allen et al., *DESI DR2 results II: Measurements of baryon acoustic oscillations and cosmological constraints*, *arXiv [astro-ph.CO]* (2025) arXiv:2503.14738.
- [106] T. Jhaveri, T. Karwal and W. Hu, *Turning a negative neutrino mass into a positive optical depth*, *arXiv [astro-ph.CO]* (2025) arXiv:2504.21813.

- [107] N. Sailer, G.S. Farren, S. Ferraro and M. White, *Disputable: the high cost of a low optical depth*, *arXiv [astro-ph.CO]* (2025) arXiv:2504.16932.